



HAL
open science

Precipitation kinetics in metallic alloys: Experiments and modeling

Alexis Deschamps, C.R. R Hutchinson

► **To cite this version:**

Alexis Deschamps, C.R. R Hutchinson. Precipitation kinetics in metallic alloys: Experiments and modeling. *Acta Materialia*, 2021, 220, pp.117338. 10.1016/j.actamat.2021.117338 . hal-03375795

HAL Id: hal-03375795

<https://hal.science/hal-03375795>

Submitted on 13 Oct 2021

HAL is a multi-disciplinary open access archive for the deposit and dissemination of scientific research documents, whether they are published or not. The documents may come from teaching and research institutions in France or abroad, or from public or private research centers.

L'archive ouverte pluridisciplinaire **HAL**, est destinée au dépôt et à la diffusion de documents scientifiques de niveau recherche, publiés ou non, émanant des établissements d'enseignement et de recherche français ou étrangers, des laboratoires publics ou privés.

Overview article

Precipitation kinetics in metallic alloys: experiments and modelling

A. Deschamps^a, C.R. Hutchinson^b

^aSIMaP, University Grenoble Alpes, CNRS, Grenoble INP, Grenoble F-38000, France

^bDepartment of Materials Science and Engineering, Monash University, Clayton, 3800 VIC, Australia

Abstract

Nanoscale precipitation is one of the most widely used microstructural tools to manipulate the properties of metallic alloys, and especially to reach high strength. Optimal microstructures are reached through complex solid state phase transformations involving non-isothermal heat treatments, metastable phases, complex chemistry, non-equilibrium vacancies, and interaction with structural defects. These phase transformations are controlled by an interplay between thermodynamics and kinetics, resulting through nucleation, growth and coarsening, in a large variety of precipitation trajectories that depend on both alloy chemistry and processing. Progress in both experimental characterization and modelling has tremendously improved the knowledge and description of these processes. The purpose of this overview is to describe the current level of understanding of precipitation kinetics, starting from the relatively simple situation of homogeneous precipitation of dilute coherent phases and including different levels of additional complexity regarding the diffusion mechanism, the effect of finite volume fraction, the effect of particle shape, the competitive multi-phase precipitation, the heterogeneous nucleation, and the non-isothermal effects.

Introduction

Solid-state precipitation is one of the most powerful means the metallurgists have at their disposal to affect the properties of engineering alloys. It is exploited in almost all alloy classes – primarily to control the mechanical properties, but it also has important effects on electrochemical properties as well as other functional properties such as the resistivity or magnetic properties. Precipitation is induced by thermal and/or thermo-mechanical treatments and controlling the precipitate nature, size, shape and spatial distribution is critical to obtaining the most desirable final properties. The process is time and temperature dependent and the microstructures obtained result from the competition between nucleation, growth and coarsening, coupled with the simultaneous competition between all possible phases (metastable and stable). This competition results in an enormous richness in the precipitate microstructures that may be obtained and this translates to a large variety in the resulting properties. It is for this reason that the solid-state precipitation processing in metallic materials attracts so much attention.

Characterizing the nanoscale precipitation process in different metallic alloys subject to the variety of thermomechanical treatments has been a constant focus in metallurgy over the past 50 years. This experimental work has been accompanied by theoretical work trying to quantitatively describe the different stages of precipitation: nucleation, growth and

coarsening, and how they interact. When combined with suitable thermodynamic and kinetic descriptions of metallic alloys, it becomes possible to build models to attempt to describe the kinetics of precipitation. These are an important and necessary component of an integrated computational materials (and process) design [1].

In recent years, the experimental techniques to characterize the precipitation kinetics in alloys have dramatically improved, now giving reasonably efficient access to the time evolution of precipitation. This characterization of transformation kinetics has been a major step forward to feed quantitative data into precipitation models, which have also developed tremendously. As a consequence, the understanding of the dynamics of precipitation reactions has now reached a much more mature level, where it can be used in more complete simulations of metal processing [2].

Although a few specialized reviews have been published in recent years addressing e.g. precipitation in Al-Cu-Li [3], in Al-Mg-Si-Cu [4], during friction stir welding of 6xxx series Al alloys [5], modelling precipitation in Al alloys [6] or nanoprecipitation and clustering in steels [7], there is no recent review addressing in a general way the question of precipitation kinetics, such as the seminal chapter by Kampmann and Wagner from 1991 [8].

Thus the aim of this overview is:

- To present briefly the different experimental techniques that can give access to precipitation kinetics: small-angle scattering, differential scanning calorimetry, resistivity, and ex-situ repeated measurements by direct observations (transmission electron microscopy, atom probe tomography)
- To present briefly the different modelling techniques that have been used to model precipitation kinetics, and their degree of maturity to describe different levels of complexity: kinetic Monte Carlo, cluster dynamics, phase field, class models, semi-analytical models
- To describe the current level of understanding, and the convergence between models and experiments, in the main situations encountered during precipitation in metals, focusing on different classes of scientific issues.

1. Experimental techniques

Characterizing precipitation kinetics means determining the evolution with time of different parameters. These include structural information (nature of the phase formed), chemical information (chemical composition, distribution of the species on the different sub-lattices of the phase), morphological information (size, shape, volume fraction), and possibly spatial distribution and orientation. Obtaining all this information in a time-resolved manner is not simple, especially when dealing with nanometer or sub-nanometer size objects, often metastable, and whose structural and chemical characteristics evolve with time.

Experimental tools can be separated into microscopy techniques, where a direct imaging of the precipitates is available, and indirect techniques, where a given signal (diffraction intensity, resistivity, heat, ...) can be converted to information regarding the precipitate state. Direct imaging techniques necessarily involve a trade-off between the spatial resolution required to determine accurately the precipitate characteristics, and the volume that can be probed, which determines the statistical relevance of the observations.

In this first section, we briefly list the main experimental techniques that can be used to access such information. We first present ex-situ techniques, whose measurements can be combined to obtain a full kinetics. We then describe in-situ techniques that can give direct access to kinetic measurements.

1.1. Ex-situ techniques

Transmission electron microscopy (TEM) and atom probe tomography (APT) are the most commonly used ex-situ characterization techniques for the study of nanoscale precipitation, and provide the largest variety of structural, chemical and morphological information. When precipitates form with a larger size (100's nm or μm 's), a larger panel becomes available, especially scanning electron microscopy (SEM), however this review will be mostly focused on precipitation at the nanoscale.

TEM provides access to the crystallographic structure of precipitates. The structure of an individual precipitate is classically evaluated by high resolution imaging: traditionally by high resolution electron microscopy, nowadays increasingly in scanning mode using high angle annular dark field (HAADF) imaging, or by combining the two [9]. Such images are inherently local (due to the necessary high resolution of the images). The challenge for obtaining kinetics from TEM is the statistical relevance of the measurements. Recent developments in scanning micro-diffraction (scanning precession electron diffraction or SPED) [10] have shown that it is possible to obtain automatically the crystal structure of very small objects and obtain an evolution kinetics for the nanoscale precipitate types [11].

TEM is particularly useful for measuring the morphological parameters of precipitates (size, size distribution, morphology, etc). Such systematic measurements have often been applied as a function of heat treatment time to obtain a set of precipitation kinetics, with the exception of the earliest stages where measurements become very tricky. Measuring a volume fraction of precipitates from TEM is somewhat more difficult, as it necessitates taking into account projection effects on the particle size distribution [12] and measuring the sample thickness, which can be achieved using electron energy loss spectroscopy (EELS) or convergent beam diffraction (CBED).

Chemical composition measurements are also possible using TEM. Semi-quantitative composition analysis can be carried out by analysis of HAADF intensity profiles, and more precise information can be gathered either by electron dispersive spectrometry (EDS) or by EELS. However, these measurements are generally quite difficult for nanoscale objects and are restricted to a limited number of objects, so they are not well adapted to the systematic measurements required for determining a full precipitation kinetics.

Although the vast majority of TEM studies provide projection images in two dimensions, it is possible to achieve 3D characterization using electron tomography [13]. A requirement is that a chemical-sensitive imaging technique is used so that diffraction effects (which have a complex orientation-dependence) are avoided.

TEM is regularly used in-situ, enabling a direct imaging of the evolution of precipitation kinetics, thus providing interesting insight on the local interactions of precipitates or transformation of the crystallographic character of individual precipitates [14]. However, one should always be aware that the observations of in-situ precipitation kinetics necessarily remain qualitative, because of surface effects on such thin samples: surface diffusion is much faster than bulk diffusion, the vacancy supersaturation will be lost more rapidly compared to bulk material, internal stresses (such as arising from coherency strains) are partially relaxed by the free surfaces, etc.

APT is the other technique of choice to obtain direct space information on precipitates [15,16]. Compared to TEM, it has less resolving power for obtaining structural information, however this is compensated by the 3D nature of the information and by the detailed information on chemistry. Recent instruments enable reconstructing volumes up to $\sim 10^6 \text{ nm}^3$, meaning that 100 precipitates can be viewed when the precipitate number density is 10^{23} m^{-3} . It therefore becomes possible to image a sufficient number of precipitates, when their number

density is large, to obtain statistically relevant information. However, many alloys possess mesoscale heterogeneities (chemical composition, distribution of structural defects, ...), which make a representative characterization by such local tools still very challenging.

Statistical treatment of the 3D datasets can provide an automated, parameter-free determination of precipitate size distributions [17]. Chemistry can be studied with a spatial resolution that allows identification of composition variations within precipitates, which has proven particularly useful to show the core-shell nature of some precipitates [18], and segregation at precipitate-matrix interfaces [19]. APT is the most sensitive technique which can reliably determine the chemistry of the residual solid solution in the matrix between precipitates, and a particularly efficient procedure to perform this measurement automatically has been devised [20]. When measuring precipitate compositions and volume fractions, APT may suffer from several artefacts, most importantly differences in evaporation fields between precipitates and matrix, preferential evaporation of some species, and more generally the effective resolution of the instrument. It is now recognized that the effective resolution of APT measurements is of the order of 1 nm [21] so that reliable quantitative characterization requires precipitates whose smallest dimension is larger than 1 to 1.5 nm, while measurements on smaller objects may remain qualitative and biased in terms of size, solvent concentration, etc.

Many other ex-situ techniques exist to provide useful information on precipitation reactions. Among the most useful, one can cite positron annihilation techniques [22,23], which provide information on the local chemical environment around vacancies, X-ray absorption spectroscopy (XAS) [24] and nuclear magnetic resonance (NMR) [25,26], which both provide information on the local environment of solute species (chemistry and structure), or thermo-electric power (TEP) [27].

1.2. In-situ techniques

Among all in-situ techniques, Small-Angle Scattering (SAS) has probably provided the most comprehensive data on precipitation kinetics. This technique can be applied with X-rays (SAXS) or neutrons (SANS) [28,29]. SAS is a diffraction technique, where the intensity scattered in reciprocal space by the precipitates depends on the contrast in scattering length density (electronic density for X-rays) between the precipitates and matrix, and on the size, morphology and size distribution of the precipitates. Recording the X-ray signal in-situ during a heat treatment allows, in principle, to follow any kind of kinetics: precipitation kinetics has been monitored from room temperature up to 1100°C for some oxide-dispersion steels [30], or in combination with plastic deformation [31] and even during welding [32]. SAS is particularly adapted to characterize very small objects, since there is no lower limit to the size it can detect. However, precipitates larger than 10-50 nm become more difficult to characterize by this technique due to the very small scattering angles involved. Some information on the chemistry of the precipitates can be obtained using contrast variation methods, such as comparing nuclear and magnetic SANS [33], combining SAXS and SANS [34–36] or changing the X-ray energy close to an absorption edge (anomalous SAXS or ASAXS) [37,38]. Limitations of SAS include the impossibility to discriminate between precipitates of different crystal structure, of simultaneously determining the precipitate morphology and size distribution, and the impossibility to determine simultaneously the precipitate chemistry and volume fraction. The lower limit in volume fraction that can be detected by SAS depends strongly on the contrast, however as a rule of thumb it lies roughly between 0.01 and 0.1 %.

When dealing with larger precipitates of significant volume fraction (>1%), in-situ X-ray diffraction (XRD) is more adapted [39–42]. It gives a more direct access to the volume fraction when the crystal structure of the precipitates is known and in cases where the material's texture is sufficiently random. It has the advantage of separating different precipitate families,

however it does not give a direct access to precipitate size. For in-situ measurements, synchrotron measurements are preferred in order to obtain a sufficient temporal resolution. SAXS and XRD signals (sometimes named WAXS for Wide-Angle X-ray Scattering when combined with SAXS) can be measured simultaneously to obtain a more complete view of reciprocal space [43–45].

Calorimetry based techniques, especially differential scanning calorimetry (DSC), are also widely used for in-situ measurements of the precipitation kinetics. DSC is very sensitive to all thermodynamic transformations, and thus provides useful information on transformations that occur during a temperature scan, such as the sequence of metastable phases succeeding each other. For a given phase, the heat signal is, at first order, proportional to the derivative of the volume fraction, so the latter can be estimated, provided that the specific transformation heat is known by other means and only one dominating precipitation reaction is occurring in a given temperature range [46]. The classic use of DSC is during heating scans at constant rate, which are very different conditions compared to more typical isothermal heat treatments. However, DSC can also be used isothermally with specific, very sensitive and stable equipment [47], and during quenching, especially since the development of ultrafast DSCs [48–50]. It can be tempting in DSC to associate individual peaks to individual structural transformations. However, one should take great care in doing so, since complex behaviors can take place in non-isothermal conditions, and the precipitation or dissolution of one phase can lead to several peaks in DSC. Since sensitive DSCs are low-temperature instruments, this technique has been mostly used for precipitation studies on light alloys such as Al or Mg based alloys.

Many other physical parameters can also be used to monitor precipitation, some of which can be measured in-situ, such as electrical resistivity [51,52]. Electrical resistivity is mostly sensitive to the matrix solid solution, so following its evolution provides indirect information on the progress of a precipitation reaction. However, below a certain size (around 1 nm), precipitates do have a significant impact on resistivity, and during the early stages of atomic clustering, the precipitation kinetics can be linked with the resistivity increase [53]. High sensitivity in-situ dilatometry can also provide information on the precipitation kinetics [54]. When studying precipitates of relatively large size (>10-100nm), 3D characterization becomes accessible using in-situ X-ray tomography [55].

2. Modelling techniques

The most commonly used precipitate kinetics models describe the evolution of precipitate number density (N) and size (R), of one or more precipitate types. Through mass conservation, they also describe the evolution of precipitate volume fraction (f_v) and solute remaining in solution, providing a range of computed parameters that can be compared with experiment. When comparing model and experiment, it is important to compare (at least) two of the above precipitate parameters, ideally those which can be measured with the greatest confidence. The focus of this section is to briefly present the most frequently used modelling techniques for simulating precipitation kinetics. The important assumptions underlying the approaches, the limitations to certain levels of complexity and the computing intensity required are discussed. The comparison with experimental measurements of precipitation kinetics under different levels of complexity is made in Sections 4-11.

2.1. Mean-field approaches – nucleation, growth and coarsening

Nowadays, by far, the most common precipitate kinetics modelling approach is the mean-field ‘class’ model for precipitation. These types of models operate at the continuum level and describe the evolution of the precipitate number density and size (assuming a certain precipitate shape) using a set of coupled evolution equations. The nucleation rate is usually described by the classical nucleation rate equation (Eq. 1) [56,57]:

$$\frac{dN}{dt} = N_{sites} Z \beta^* \exp\left(-\frac{\Delta G^*}{kT}\right) \quad [1]$$

N is the number of precipitates per unit volume, t is time, N_{sites} is the number of sites per unit volume where nucleation can take place, Z is Zeldovich’s factor, accounting for the fluctuations of clusters at the critical size, β^* is the critical attachment rate of a solute on a precipitate at the critical radius, ΔG^* is the all-important nucleation barrier and kT is the thermal energy. Detailed expressions for Z and β^* have been derived and can be found in [58].

The classical nucleation rate equation was originally derived for condensation of liquid droplets from vapor and has been adopted for use in solid-state precipitation reactions, even though in its most commonly used form, it is only applicable for precipitates forming with the same composition as the matrix and where the rate limiting step is the interfacial attachment of atoms. ie. there is no chemistry change. The assumptions underlying Eq. 1 are strong and there have been many attempts to build on Eq. 1 and relax some of these constraints. These approaches, and the limitations of Eq. 1, are discussed and summarized in [59].

The growth rate of spherical, solute-rich, precipitates, is usually described by a form of Zener’s diffusion-controlled growth solution (Eq. 2) [60], made under hypothesis of a binary system, of quasi-stationary growth, of a composition-independent diffusion coefficient and a small supersaturation:

$$\frac{dR}{dt} = \frac{D}{R} \left(\frac{C_{mf} - C_e^R}{C_\beta - C_e^R} \right) \quad [2]$$

R is the radius of the growing spherical precipitate, D is the diffusivity of the rate controlling species in the matrix, C_{mf} is the concentration of solute in the mean-field matrix, C_β is the solute content inherited by the precipitate for the increment of growth dR (which may not be constant), and C_e^R is the solute content in the matrix at the precipitate-matrix interface, which is usually taken as the local-equilibrium composition corrected for the Gibbs-Thomson effect.

When Eqns. 1 and 2 are numerically integrated and the evolution of the full particle size distribution is monitored, we refer to it as a ‘class’ model. Such a model was first introduced by Kampmann and Wagner [8,61] and is sometimes referred to as the Kampmann-Wagner N (numerical) model. Numerically, the precipitate size distribution is discretized into classes and the evolution of the distribution can be described either with a Lagrangian-type approach where the size of a precipitate class evolves with time, or an Eulerian-type approach where the size of precipitate classes is fixed and precipitates change classes during growth or dissolution [62].

A particular advantage of class models for spherical precipitates is that coarsening is naturally captured through the Gibbs-Thomson effect in Eq. 2 (C_e^R) and no further equations are required. Despite the simplicity, these types of class models have been remarkably successful and can show a large richness in behavior when coupled with reliable thermodynamic and kinetic databases. Due to this success, class models for precipitation are now integrated into commercial software such as TCPrisma, MatCalc and PanPrecipitation, which no doubt

enhances their popularity [63–68]. We will show a number of examples of the success of class models in the following sections.

With modern computers, the computational cost of a class model of precipitation is no barrier to implementation and they can be easily implemented on modern laptops. This was not always the case. In the past, approaches that describe the precipitation kinetics using Eqns. 1 and 2, but which monitor only the mean precipitate size (\bar{R}) instead of the full size distribution were popular and computationally much lighter, e.g. [69]. These ‘mean radius’ approaches require an explicit description for the coarsening stage of precipitation, as well as a criterion to describe the transition from the growth state to coarsening. Coarsening in such models is usually described using the Lifshitz-Slyozov-Wagner (LSW) equation derived for dilute solutions (Eq. 3) [70,71]:

$$\bar{R}_t^3 - \bar{R}_0^3 = \frac{8D\gamma C_{mf} V_m^2 t}{9R_g T} \quad [3]$$

γ is the interfacial energy of the precipitates, V_m is the molar volume, and R_g is the gas constant. The mean field solute concentration in the coarsening stage is in local equilibrium with the precipitates of mean size, and equals the equilibrium concentration when the Gibbs-Thomson effect becomes negligible.

Whether it is a class model, or the mean particle size model which is used, there are a large number of assumptions that lie behind Eqns 1-3 when used in mean field models, and which are not frequently discussed. These models are mean-field models, meaning there is no direct interaction between precipitates, and they only interact with the surrounding matrix of a mean-field solute composition. This approximation improves as the volume fraction of precipitates approaches zero (dilute approximation) and the important effects of a finite volume fraction (non-dilute solutions) is explored in Section 6 of this overview.

To make the calculations, we must know the interfacial energy (γ) and Gibbs energy of the precipitate phase(s) (as well as the matrix phase) which may change with size, temperature and composition. These are required for the calculations of the all-important energy barrier for nucleation, ΔG^* , but also the solute concentration at the matrix/precipitate interface, C_e^R , that affects the growth and coarsening kinetics. Whilst these important thermodynamic parameters may be well defined for large particles, when the particles are of the order of 1nm or less, the situation is much less clear and the nucleation rate is especially sensitive to their effect on ΔG^* . The structure and chemistry of the newly forming precipitate may be significantly different from that expected at equilibrium, and the effective interfacial energy may show an important size and chemistry dependence. These questions also depend on exactly how we define a precipitate at these small length scales and these questions are explored in Section 3.

In addition to thermodynamic descriptions of the precipitating system, calculations also require accurate kinetic information in the form of diffusivities (D) or mobilities (M). In many cases, particularly at low temperatures, non-equilibrium vacancy concentrations can be present during precipitation leading to enhancements in the diffusivity that may show a time-dependence even under isothermal conditions. Vacancies may also preferentially interact with solutes in solution leading to trapping effects, or correlations, leading to other types of deviations in the diffusivities. Such effects have been experimentally observed and they are explored in Section 5 of this overview.

The use of the classical nucleation equation (Eq. 1) requires one to know the number of available nucleation sites (N_{sites}) as well as the nucleation barrier (ΔG^*) applicable at those sites. One differentiates between ‘homogeneous’ nucleation, where all sites in the matrix are considered equally probable and the available number of sites is approximated by the number of lattice sites, or ‘heterogeneous’ nucleation where particular sites, such as dislocations, solute clusters, grain boundaries, are preferred sites. There are a few cases where the homogeneous nucleation model may be a reasonable approximation and these are discussed in Section 4. However, heterogeneous nucleation tends to dominate in engineering alloys, and a particular challenge is calculation of the nucleation barrier at these heterogeneous sites. Heterogeneous precipitation is explored in Section 10 and the related topic of metastable phases and ‘precipitation trajectories’ is explored in Section 9.

The mean field framework described above does not require the precipitate to have a constant composition during precipitation, but this is the way it is usually treated in kinetic models. There is increasing experimental evidence that a constant precipitate composition is actually rare and this evolution in composition affects all aspects of the nucleation, growth and coarsening behavior. The effects of precipitate non-stoichiometry are discussed in Section 7.

The equations above, used in mean-field models for precipitation kinetics, are written assuming spherical precipitate shapes. Indeed, they assume a shape and that the shape does not change during growth or coarsening. These models do not describe morphological transitions. Whilst spherical precipitates do exist in some alloy systems, and some of these will be discussed in Section 4, it is more common for precipitates to be non-spherical: plate and rod-shaped precipitates are common. In these latter cases, Eq. 2 can be replaced with the Zener-Hillert equation for the shape-preserved lengthening rate (Eq. 4) [72–74] in the mean-field models but such equations cannot self-consistently also describe coarsening and there are many further complications in trying to simulate non-spherical particles. The important considerations for non-spherical particles are discussed in Section 8 of this review.

$$\frac{dL}{dt} = \frac{D}{\alpha} \left(\frac{C_{mf} - C_e^r}{C_\beta - C_e^r} \right) \quad [4]$$

L is the precipitate plate or rod length, $\alpha=r$ for rods and $2r$ for plates, where r is the rod or plate lengthening tip radius.

2.2. Cluster Dynamics

A closely related mean-field class model that can also be used to describe precipitation reactions is Cluster Dynamics. The precipitates are described by a single variable, the number of atoms they contain, and they grow or shrink by exchanging atoms with the surrounding mean field. The evolution of the precipitate size distribution is described by a master equation, Eq. 5 [75–77]:

$$\frac{dC_n}{dt} = \alpha_{n+1}C_{n+1} + \beta_{n-1}C_{n-1} - (\alpha_n + \beta_n)C_n \quad [5]$$

C_n is the concentration of n sized clusters, α_n is the evaporation rate which describes the probability of a n -sized cluster to release an atom into the mean field per unit time, and β_n is the growth rate which describe the probability the n -sized cluster will add an atom from the mean field per unit time.

The growth rate, β_n , is derived assuming long range diffusion control, and the evaporation rate, α_n , by assuming detailed balance between growth and shrinkage, requiring a precise description of the volume and surface contributions to the clusters' free energy. A detailed derivation is given in [75] and the growth and evaporation rates must be carefully defined with respect to the thermodynamics and kinetics of the system being studied. The particle size distribution is discretized into size classes and the movement between size classes is described by Eq. 5.

Cluster Dynamics differs from the 'nucleation and growth' class models described above in the sense that there is no explicit nucleation stage or nucleation description such as in the CNT. No barrier for nucleation needs to be defined. Indeed, no explicit differentiation is made between the product and matrix phase, and no critically sized nuclei is defined. The state of the system is simply defined by the cluster size distribution and this will include sub-critically sized clusters when comparing with the CNT framework. There are some advantages to such an approach when comparing with experimental measurements and this is discussed in Section 3.

2.3. Full-field approaches – Phase field simulations

The mean field approximation in modelling precipitation kinetics is convenient from a computational viewpoint but it is a quite strong assumption. The mean field approaches cannot capture precipitate interactions other than the indirect effects through the mean field, cannot describe morphological transitions, they are not well suited to the commonly observed non-spherical precipitate shapes and cannot describe well the coarsening stages for such distributions. The alternative is a full field approach, such as Phase field. Phase field simulations are also continuum approaches describing precipitation by coupled field-equations but they do not *a priori* assume the precipitate shape. Instead, the shape is a consequence of anisotropy in migration rates of different precipitate interfaces which occur in response to anisotropies in interfacial energy and interfacial mobility, and local elastic or chemical fields. When phase field simulations are properly coupled with reliable thermodynamic and kinetic databases, they can describe the evolution of a precipitate distribution during growth and coarsening, taking into account variations in particles shapes and interactions between particles ; examples include the description of precipitation in Ni-based alloys [78–80]. They can naturally describe coarsening in a system of non-spherical particles. In principle, defects in the form of heterogeneous nucleation sites could also be introduced into phase field simulations of precipitation. The flexibility of phase field simulations comes with much greater computational cost, especially when extended to 3D. Phase field simulations cannot naturally simulate nucleation. Nucleation is incorporated manually using either noise, or a form of the classical nucleation equation (Eq. 1). Some examples of the power of this full-field approach for describing precipitation processes in topologically complex systems is shown in Section 8. Excellent reviews of the phase field method exist and the interested reader is referred to the following [81,82].

2.4. Atomistic approaches – Lattice Kinetic Monte-Carlo (LKMC)

The continuum models for precipitation (mean-field or full-field) are efficient for describing the growth and coarsening regimes of precipitation where mass transport occurs over relatively long times and distances in the microstructure.

However, at the very earliest stages of precipitation, including the nucleation stage, atomistic approaches can provide important new insights. Molecular Dynamics (MD) does not allow access to the necessary timescales to be able to describe the chemistry changes associated with solid state precipitation in most engineering alloys, but a number of authors have successfully used Lattice Kinetic Monte Carlo (LKMC) approaches to simulate precipitate nucleation and early-stage growth. The downside of LKMC is that due to the computational demands it is limited to short aging times and large supersaturations, and can only be applied to coherent phase formation where the structure of the precipitate can be expressed in terms of the underlying lattice of the matrix. This is a strong constraint. The formation of L1₂ ordered phases in a FCC matrix is such a case and this example will be shown in Section 4.

The simulation usually considers a rigid matrix lattice (although approaches that include relaxation do exist) and the atoms are constrained to occupy sites on this lattice. The thermodynamics of the system is represented by a bond energy summation (E) over the system (Eq. 5)[58,83,84]:

$$E = \frac{1}{2N_s} \sum_{i,j}^{n,m} \varepsilon_{ij}^1 p_n^i p_m^j + \frac{1}{2N_s} \sum_{i,j}^{r,s} \varepsilon_{ij}^2 p_r^i p_r^j \quad [5]$$

N_s is the total number of lattice sites in the simulation box and p_n^i is an occupation number with $p_n^i = 1$ if site n is occupied by an atom of type i and $p_n^i = 0$ if not.

The first and second summations apply to the first and second nearest neighbors pairs of atomic sites, and $\varepsilon_{i,j}^1$ and $\varepsilon_{i,j}^2$ are the effective energies of the pairs of sites. All of the thermodynamic properties lie in the first and second nearest neighbor interaction energies and these must be chosen carefully to properly reproduce the thermodynamic properties of the alloy of interest. Depending on the system, higher order terms may be required.

For diffusion mediated by the vacancy mechanism, a single vacant lattice site is introduced in the simulation and atoms may exchange positions with the vacancy with a certain attempt frequency that depends on the energy required to move the atom from its current lattice site, to the saddle point between it and the vacancy. In this way, the atomic configuration of the system evolves by subsequent jumps of the vacancy. No assumptions need to be made about the shape of the precipitate and no choices need to be made regarding the interfacial energy, or its size dependence – these are naturally captured in the bond energy summations. The LKMC approach is simple in principle but great care must be taken in correctly identifying the thermodynamic and kinetic input parameters.

This powerful approach has been used to simulate the initial ‘homogeneous’ nucleation and early stage precipitate growth and examples will be discussed in Sections 4 and 7. The major limitations are the computational cost which restricts LKMC to short aging times and to large supersaturations, and the need to describe the crystal structure of the precipitate in terms of the underlying matrix lattice.

The following sections address different cases of precipitation, first providing experimental evidence of the main points to be discussed, and then details on how the different phenomena are taken into account in the models. Each section concludes by summarizing the current limitations of the understanding / experimental description / modelling.

3. Definition of precipitates

Before discussing in detail the kinetics of precipitation, it is useful to discuss the definition of a precipitate. In the common sense of metallurgists, precipitates are defined by a specific crystal structure, and this translates thermodynamically into a specific relationship between chemical composition and energy, which is usually described in thermodynamic databases by the Gibbs energy of the phase. Usually, an assumption lying behind precipitation models is that a collection of precipitates of the same phase existing in a microstructure share common features: at a given ageing time, they all have the same chemical composition and the same interfacial energy with the matrix, i.e there exists a precipitate size distribution but not a precipitate composition distribution among a given phase. Such definitions are well suited to relatively large precipitates that are found in late stages of precipitation processes. However, when considering precipitates from the atomic scale, and hence describing the early stages of precipitation, arriving at a clear definition of a precipitate is less clear. In the initial stages of clustering, the typical size of solute-rich features is commonly sub-nanometric [85]. An example of clusters formed from natural aging of an Al-Mg-Zn alloy is shown in Fig. 1. In such cases, it becomes difficult to uniquely define precipitates: their chemical composition is ill defined, their interface with the matrix may be far from a well-defined surface, and their crystal structure can exhibit different partial degrees of ordering existing in different objects. Although such clusters are still in many cases considered as individual objects, e.g. in APT volume analyses, their distribution may be more suitably described as fluctuations of concentration in solid solution, in a way similar to the description of spinodal decomposition [36,86]. Obviously, such a description poses the question of how to deal with the transition to more classical descriptions of precipitates during later stages of phase transformations.

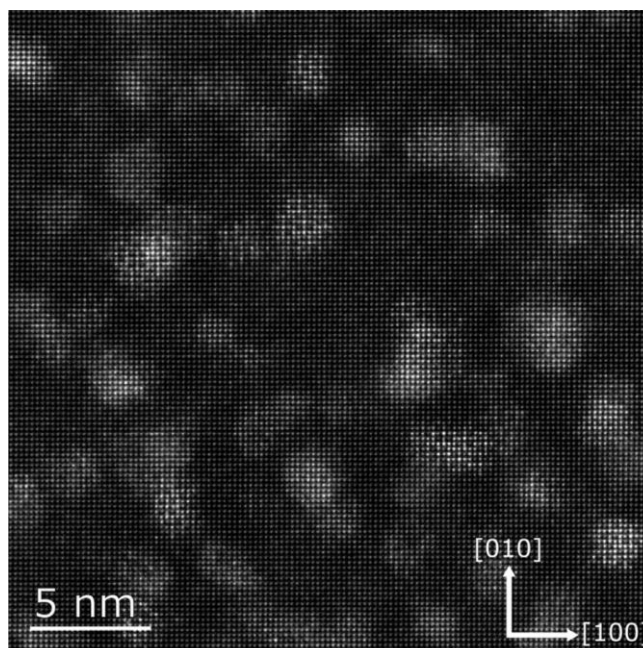


Figure 1: HAADF imaging of clusters in Al-Mg-Zn after natural ageing. From [87].

Aside from the question on the definition of a precipitate, a related question when comparing experiments and models is the detection of these objects, which should be made with the same criteria in experiment and model. In many microscopy observations, the detection of precipitates is limited by resolution, and/or by the contrast, so that small clusters that are close to the matrix in both composition and structure may not be detected. On the other hand, in the classical framework of precipitation modelling, the distinction between a sub-critical

cluster and a precipitate is defined by the critical nuclei size. The two definitions agree only if the detection limit for microscopy coincides with this critical size. Differences between these two criteria may lead, e.g. to systematic biases in nucleation rates. Small-Angle Scattering, which is able to resolve fluctuations of chemical composition at sub-nanometric scale, does not make any differentiation between sub-critical clusters and precipitates and provides a global measurement of all features present in the microstructure. Such data could be advantageously compared with Cluster Dynamics simulations, that do not require the definition of a critical nuclei size. This experimental detection of subcritical clusters is probably one reason why in most published precipitation kinetics using in-situ SAS (e.g. [37,88–90]), the number density of precipitates is only observed to continuously decrease, i.e. no apparent nucleation takes place, simply because in the very early stages, sub-critical clusters are included in the analysis, whose number is constantly decreasing with time. An example is shown in Figure 2, showing in-situ SAXS measurements of precipitation in a Zn-Al-Mg alloy. There is no obvious domain where the number of particles is increasing.

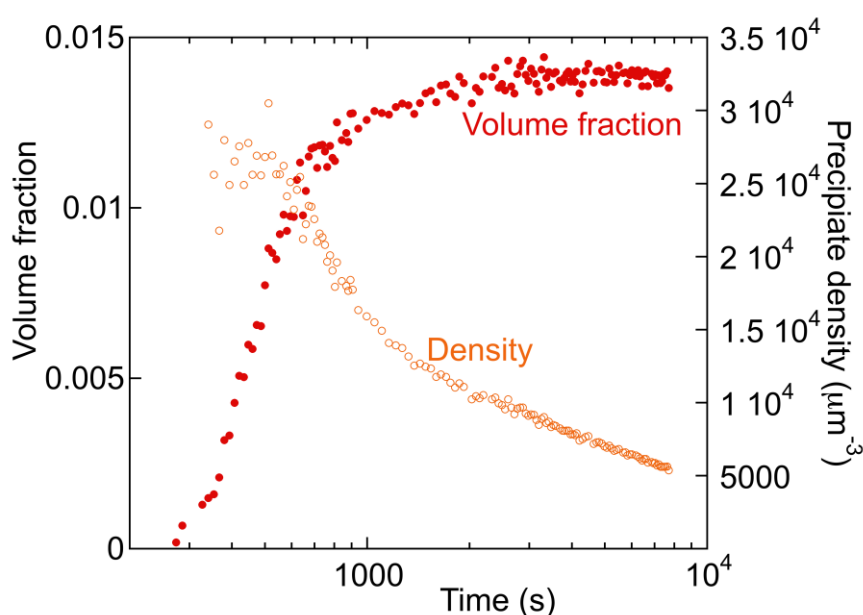


Figure 2: Evolution of precipitate volume fraction and number density from in-situ SAXS measurements on a Zn-Al alloy aged at 95°C – from [88].

When dealing with these early stages of precipitation, it therefore becomes necessary to define frameworks that allow a sound comparison, both between different experimental techniques and between experiments and the outcomes of models. Such common frameworks are being developed actively, e.g. to compare SAS and APT [21], or to define in a parameter-free way a distribution of precipitate sizes from APT measurements [17].

Another issue when dealing with the thermodynamic description of precipitates, especially when modelling is involved, is the implicit homogeneity of the structure and chemical composition of the phases which is usually assumed by models working at the continuum level. It is now experimentally well established that many (if not most!) precipitates show some heterogeneity, such as a core-shell chemical structure or complex structure and distribution of chemical species at the interface, which may represent a large fraction of the precipitate's atoms. Such features are still very challenging to describe in many modelling frameworks.

4. Homogeneous precipitation of dilute, stoichiometric, spherical phases during isothermal treatments.

In the simplest, idealized situation, precipitation occurs within a perfect lattice (i.e. without interference from crystalline defects such as grain boundaries and dislocations) by forming particles of second phase of a given crystal structure and homogeneous chemical composition, of small volume fraction (dilute limit). In this case, one can consider that the interaction between particles occurs only through the solid solution composition present between the precipitates, considered spatially uniform except close to the particles, which makes it possible to apply a mean field approach to precipitation kinetics. This idealized situation is very difficult to find in practice: when only a very small fraction of precipitates is formed, the supersaturation is usually small, which favors heterogeneous nucleation. In order to maximize the supersaturation while keeping the precipitate fraction small the solubility of the precipitate-forming solute should be as small as possible.

In this idealized situation, the description of precipitation kinetics is summarized by the description of the evolution of the precipitate size distribution, under the strong hypothesis that all precipitates of a given size (i.e. a given number of atoms) have the same thermodynamic properties, namely volume and surface free energies, and that diffusion occurs exclusively by monomers (i.e. isolated solute atoms).

In such a simplistic situation, the classical nucleation theory (Eq. 1) has been applied with some success [58,91,92]. The nucleation driving force can be obtained directly from thermodynamic databases or calculated by appropriate thermodynamic models such as cluster variation methods (CVM) [92]. These calculations show that care needs to be taken when using simple expressions such as regular or ideal solution, which in general do not lead to a reliable expression of the driving force.

Even for the simplest case of spherical precipitates, a reliable description of the interfacial energy of the small particles that are involved in the nucleation process necessitate to take into account a size dependence of γ , as well as a temperature dependence [75]. Taking into account the influence of points and lines in the description of a spherical interface, an approximation valid for precipitates larger than a few atoms is:

$$\gamma = \gamma_0(1 + c n^{-1/3} + d n^{-2/3}) \quad [6]$$

where n is the number of atoms per cluster, c and d are constants that represent the line and point contributions and γ_0 is the interfacial energy for large precipitates.

An example where a good level of description has been reached is the precipitation kinetics of $L1_2$ ordered precipitates in Aluminum, and particularly the Al_3Sc and Al_3Zr phases. Although the latter is a metastable phase, it is observed in practice even at low supersaturation. These two systems represent good model systems thanks to the limited existence of elastic stresses (related to the small difference of lattice parameters between the precipitates and matrix), the low solubility of Zr and Sc in Al, and the spherical character of the precipitates. In such systems the interfacial energy, whose value dramatically affects the nucleation rate, is dominated by the chemical component and this can be calculated with good precision. Nucleation rates from CNT are consistent with those obtained from kinetic Monte Carlo modelling [58,75,92], Fig. 3.

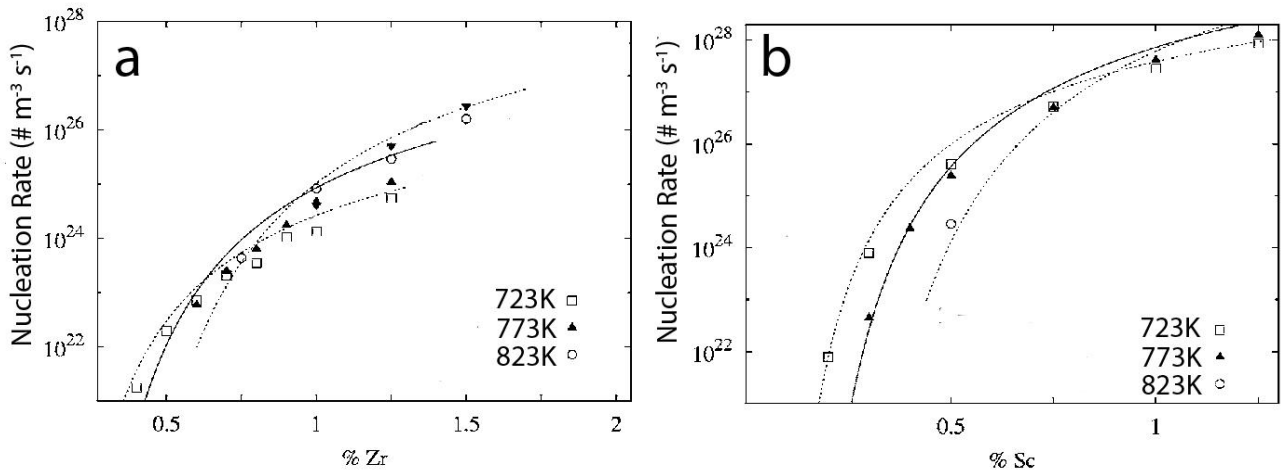


Figure 3: Comparison of the steady-state nucleation rate of L12 precipitates in FCC Al calculated using classical nucleation theory (lines) and kinetic Monte Carlo (symbols), as a function of a) Zr content, and b) Sc content at a range of temperatures. Modified from [92].

In such systems, the description of later stages of precipitation, i.e. growth and coarsening, can be achieved relatively straightforwardly using Eq. 2 implemented in the mean-field class models described in Section 2.

This precipitation kinetics shows typically four different stages:

- i- nucleation, where the precipitate size is constant and the precipitate density quickly increases. Although this stage is observed in models, it is rarely found in experiment, as discussed in Section 3 (Fig. 2);
- ii- growth, where the number density of precipitates is constant and the precipitate size rapidly increases, and becomes much larger than the critical radius. This is the stage where all precipitates in the distribution grow together. At the end of this stage, the diminishing supersaturation causes the critical radius to increase and to enter in the particles size distribution range, so that the smallest precipitates become unstable;
- iii- transition between growth and coarsening, where the microstructure seems stable, with a constant average precipitate radius. During this stage, the particle size distribution shape evolves, becomes wider, as the smallest precipitates start to dissolve, yet are still present, which compensates the increasing size of the largest precipitates [62].
- iv- coarsening, where a self-similar particle size distribution is reached, the average and critical radii grow together, and the precipitate number density decreases. The precipitate volume fraction is equal to the Gibbs-Thomson corrected equilibrium fraction, which might in cases of small precipitate size and high interfacial energy still be significantly different from the final equilibrium fraction.

Using a mean field nucleation and growth class model of the Kampmann-Wagner type (Eq. 1 and 2) leads naturally to the classical coarsening LSW law (Eq. 3), and its time exponent of $1/3$, in agreement with experimental data [37]. Although the agreement between models and experimental data concerning the time exponent for coarsening is good [62], most experimental determinations of the particle size distribution during coarsening do not agree with the theoretical LSW shape [62], with a few exceptions which are compatible within experimental uncertainty [93]. Generally, experimentally determined particle size distributions are much closer to a log-normal distribution with the presence of large precipitates, whereas the LSW distribution predicts a cut-off radius.

In addition to the now common mean-field class models for precipitation, one can obtain similar results during isothermal ageing by other modelling methods, such as the mean-radius

approach or Cluster Dynamics. Although the mean radius approach is less versatile than the class methods, it requires much less numerical resources which can make them more appropriate to couple with process control or other models such as finite element modelling, and provides identical results to class models in simple situations. An example is shown in Fig. 4.

Cluster dynamics models have also proven efficient to describe precipitation kinetics and compare well with other methods [75,94]. As can be seen below in Fig. 4, they have the advantage of being able to access much longer time frames than KMC, but do not need to explicitly invoke a nucleation stage like traditional class models.

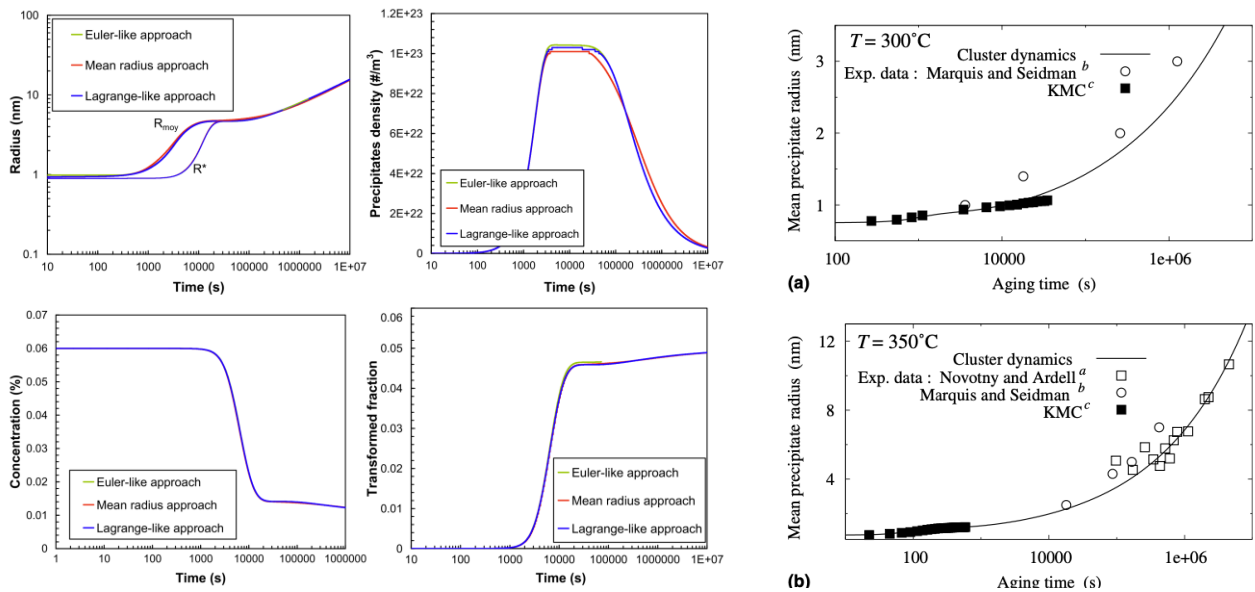


Figure 4: Left: Comparison between two types of class modeling approaches (Eulerian and Lagrangian-type) and a mean radius approach for modelling a complete isothermal precipitation kinetics (from [62]); right: simulation of precipitation kinetics in Al-Sc at two temperatures using LKMC and CD, compared with experimental data (from [75]).

The alloy systems that are relatively close to the idealized situation invoked in this section are not very numerous. One can cite studies of Al_3Sc and Al_3Zr in Al, Co in Cu [89], Fe_2SiTi in Fe [95] (although in the two last cases the volume fraction is too high to really satisfy the dilute approximation). Of particular interest to evaluate the capability of the current state of modelling to describe experimental data are high throughput experimental approaches such as carried out on Cu-Co [89], which involves space- and time-resolved SAXS experiments on compositionally graded alloys, covering a range of compositions. The full set of compositionally-dependent precipitation kinetics at three temperatures could be described by a class model, with a limited number of parameters. However, the description of the early stages of precipitation was still far from satisfactory, showing that there is still much room for improvement in our description of the nucleation stages of precipitation in metallic alloys [59].

5. Influence of the diffusion mechanisms on precipitation kinetics

Precipitation involves the movement of solutes. In metals, most solutes forming precipitates are substitutional and thus the diffusion mechanisms involve mainly the movement of vacancies. Therefore, the precipitation kinetics is directly controlled by the concentration of vacancies by their diffusion rate within the material and by their interaction with solutes [96–98,36,99,100]. An important exception is the precipitation of cementite in steels during

martensite tempering, where carbon diffuses interstitially. However, in many cases, cementite precipitation can be accompanied by concurrent substitutional solute partitioning which occurs by a vacancy mechanism [101,102].

During precipitation, the concentration of vacancies is generally out of equilibrium. This happens, e.g. during quenching where temperature changes too rapidly for the vacancies to equilibrate [103,104], or during early precipitation stages after quenching where an excess vacancy concentration is retained. Knowing the magnitude of this vacancy excess and its evolution during precipitation is a difficult task. In most cases, it has been neglected by models, which is probably a good approximation at relatively high temperatures where the excess may rapidly annihilate, but not during early processes such as formation of GP zones or clusters close to room temperature. At these lower temperatures, there is conclusive evidence that it plays a prominent role [105,106]. There are few experimental techniques capable of measuring vacancy contents quantitatively. Positron annihilation can be used although great care must be taken in the quantification process [107]. An example of the positron lifetime measured in an Al-Mg-Si alloy as a function of natural ageing time at room temperature after quenching is shown in Fig. 5. Whilst the three different quenching processes (IWQ, VC and AC) lead to the same positron lifetime at long times, the early time differences (<30min) are attributed to different vacancy and clustering states.

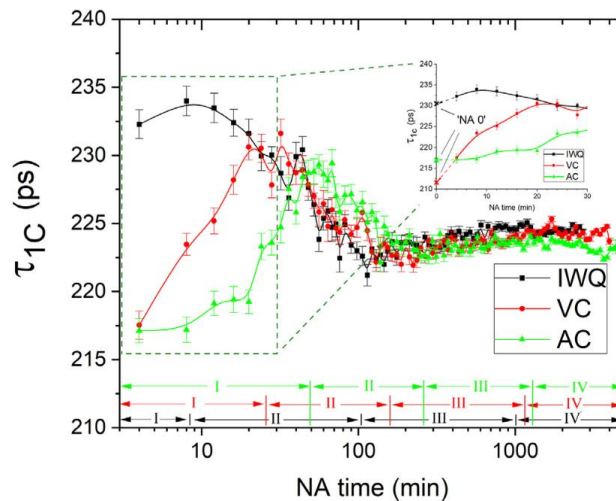


Figure 5: Positron lifetime evolution during natural ageing of an Al-Mg-Si alloy after different quenching procedures from solution treatment. The early time difference results from very different vacancy concentrations and clustering states (from [106]).

Another key issue to consider is the interaction of vacancies with solutes, and frequently with solute clusters. In some systems, it can be a good approximation to consider that single vacancies exchange with single solutes without special correlative effects. In this case, models considering the diffusion of single solutes as controlling precipitation are realistic. However, it has been shown by atomistic modelling that this approximation breaks down in a number of cases. A good example of more complex diffusion pathways happens during Cu precipitation in Fe, where a significant transport of solute happens by diffusion of dimers or trimers, which has consequences on the description of the precipitation kinetics [94,108,109].

It is also well known that the removal of solute from the matrix in Al alloys during low temperature clustering (natural ageing) shows a logarithmic time dependence, rather than the power-law kinetics that would be expected for a diffusion controlled process [53,110,111]. This has been interpreted in terms of the preferred interaction between vacancies and solute atoms and the temporary trapping of vacancies at clusters (using the so-called vacancy-pump model [112]). Another complexity arises when correlations between

vacancy movements and solutes result in the displacement of groups of solute atoms, which can involve as much as the displacement of whole precipitates, thus favoring precipitate coagulation [113].

Last, the diffusion mechanism may become complex in multi-component alloys and influence significantly the precipitation pathway. This happens when complex solute-vacancy binding effects occur, resulting in cross-terms in the Onsager diffusion matrix, and therefore to coupling of solute fluxes during the precipitation process [113,114].

6. Effects of finite volume fraction

Most practical cases where precipitation kinetics is studied involve volume fractions that are too high to satisfy the dilute approximation. If we approximate the distance between precipitates as $d = \left(4\pi/3f_v\right)^{1/3} r$, where r is the precipitate size and f_v is the precipitate volume fraction, the limit for dilute approximation can be placed somewhat arbitrarily when the ratio d/r is between 5 and 10, corresponding to a volume fraction of 3 to 0.4% respectively. However more restrictive definitions exist, and show that deviations from the dilute approximation may exist as early as a solute fraction of 0.1% [58].

In a non-dilute system, most hypotheses that underpin the ideal description of precipitation kinetics described in Section 4 become invalid. Starting with nucleation, the free energy of clusters preceding precipitation is modified by cluster interactions. In a non-dilute system, one has to take into account the probability of cluster coagulation, and the geometrical frustration, which means that the available volume to nucleate a cluster is the free volume unoccupied by existing clusters. Modifications have been made to account for these effects and the new equations have been successfully compared to cluster size distributions and nucleation rates predicted by Monte Carlo simulations [115–117], applied to a good model system namely the formation of Al_3Li precipitates in Al: spherical coherent precipitates, low coherency strains, volume fraction up to 20%.

During the later stages of precipitation, the increase of volume fraction has a number of consequences. When increasing supersaturation, models show that the different stages of precipitation, namely nucleation, growth and coarsening, become increasingly overlapped, meaning in particular that no distinct growth stage can be defined [118].

Most importantly, the breakdown of the dilute approximation results in the breakdown of the mean field approximation, meaning that the evolution with time of a single precipitate does not depend only on the average microstructure (matrix solute content and particle size distribution) but also on its neighbors. A small precipitate that should dissolve due to the Gibbs-Thomson effect may actually grow if it is surrounded by even smaller precipitates. A second related consequence is that the diffusion fields in the matrix surrounding growing or shrinking precipitates may overlap, which increases the kinetics of solute transport between precipitates in the coarsening stage. The extreme case is when precipitates can touch each other, which may lead to coagulation [113], and whose effect on the kinetics of microstructure evolution has been modelled in Ni superalloys [119].

These correlation effects are most pronounced during the coarsening stage. Indeed, during the growth stage the solute flux happens mainly from the supersaturated solid solution towards the precipitates, so that neighboring particles are shielded by this supersaturation. During coarsening, however, the solute movement consists of exchanges between precipitates and thus involves much more dramatic spatial correlation effects. Considerable work has been published to establish corrections to the classical dilute approximation LSW theory of coarsening [120–126], e.g. Fig. 6. As the volume fraction of particles increased, the

acceleration of the coarsening rate constant, compared with the dilute limit LSW value, can increase by an order of magnitude.

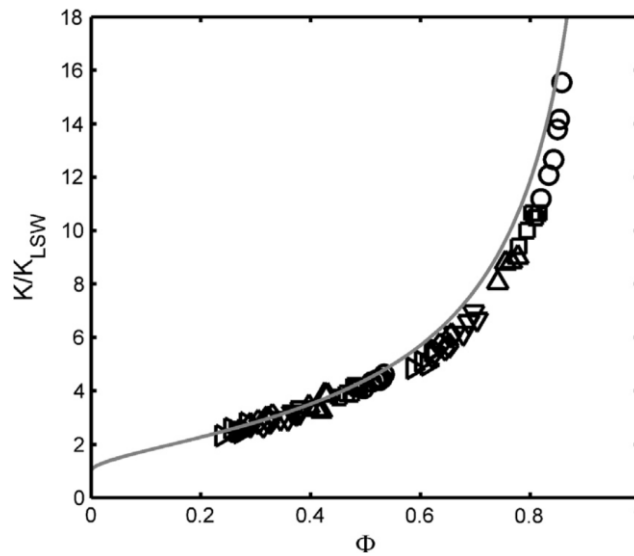


Figure 6: Effect of volume fraction ϕ on the coarsening rate constant K normalized by the dilute limit coarsening constant K_{LSW} predicted by modelling (from [125]).

7. Non stoichiometric precipitates

In most practical situations, it is not a good approximation to assume the precipitates have a constant composition throughout the precipitation process. Since the development of appropriate measurement tools, of which Atom Probe Tomography is the most illustrative, it is now known that particles are found to be much richer in the solvent species than the equilibrium value during the early stages of precipitation. In precipitates containing several solute species, the ratio between these species usually evolves with time. There can be several reasons for these deviations from stoichiometry.

7.1. Non-stoichiometry may help nucleation.

The CNT nucleation barrier is proportional to $\gamma^3/\Delta g_v^2$, and deviations from stoichiometry affect both the interfacial energy (γ) and the nucleation driving force (Δg_v).

When compared to a stoichiometric precipitate, the formation of a particle with a higher solvent concentration will increase its volume free energy but simultaneously decrease the chemical contribution to the interfacial energy. It is frequently favorable to accept this deviation from equilibrium during early precipitation stages [127,128]. Formation of a nuclei with a composition closer to the matrix composition also offers kinetic advantages since less long-range mass transport is required. This precipitation pathway, starting from very dilute precipitates, which become more concentrated in solute over time, sometimes called non-classical nucleation, can be quite similar in some aspects to spinodal decomposition, making the two difficult to distinguish from the perspective of the increase with time of the concentration contrast within the alloy.

In other cases, the precipitate composition that gives a maximum in the nucleation driving force may differ substantially from the equilibrium composition of the bulk precipitate. This can occur especially in cases where the precipitate contains more than one type of solute. In such cases, there can be a large bias between the precipitate composition at early and late stages of precipitation. A good example is the nucleation of V(C,N) in steels, where the C/N

ratio at nucleation is very different from the equilibrium bulk precipitate value [129], see Fig. 7.

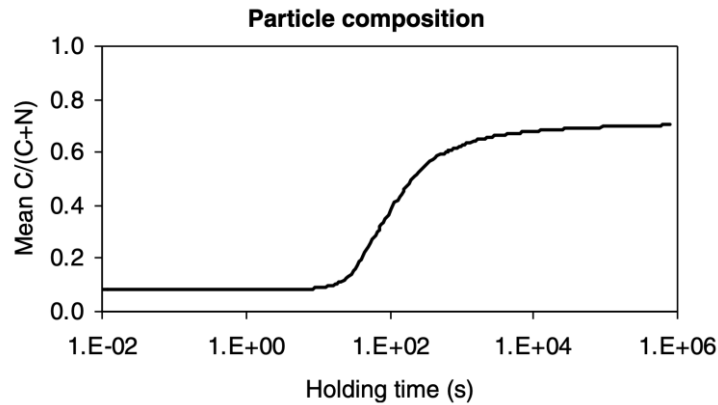


Figure 7: Predicted evolution of relative carbon content in $V(CN)$ precipitates during precipitation in Fe, showing a large deviation from equilibrium in the early stages that helps maximizing the nucleation driving force (from [129]).

7.2. Non-stoichiometry due to large differences in solute diffusivities

When large differences in diffusivities exist between the different solute species, faster growth can occur by maximizing the concentration of fast-diffusion solute, resulting in concentration changes during the course of precipitation [37]. When precipitates dissolve, the reverse can occur, namely the fast diffusion species leaves first, which increases the concentration of slow diffusing species in the precipitates [130]. A particular case of this evolution of precipitate composition with time is when vacancies do not enter frequently in the precipitates, in which case the precipitates conserve the history of the different layers of solute that have been added with time, resulting in a core-shell precipitate structure [84]. This formation of core-shell structures is exemplified in aluminum alloys by the many possible substitutions in the L_{12} structures: most classically Sc and Zr, but also Ti, Er, V, ... [131–134]. An example of such a core shell structure in Al-Sc-Zr is shown in Fig. 8 below. The role of this shell may also be to decrease the interfacial energy between the precipitates and matrix [135]. This core-shell structure may result in a relatively fast rate of formation of the precipitates (controlled by the fast diffuser) followed by an extremely slow coarsening rate (controlled by the slow diffuser) [136,137].

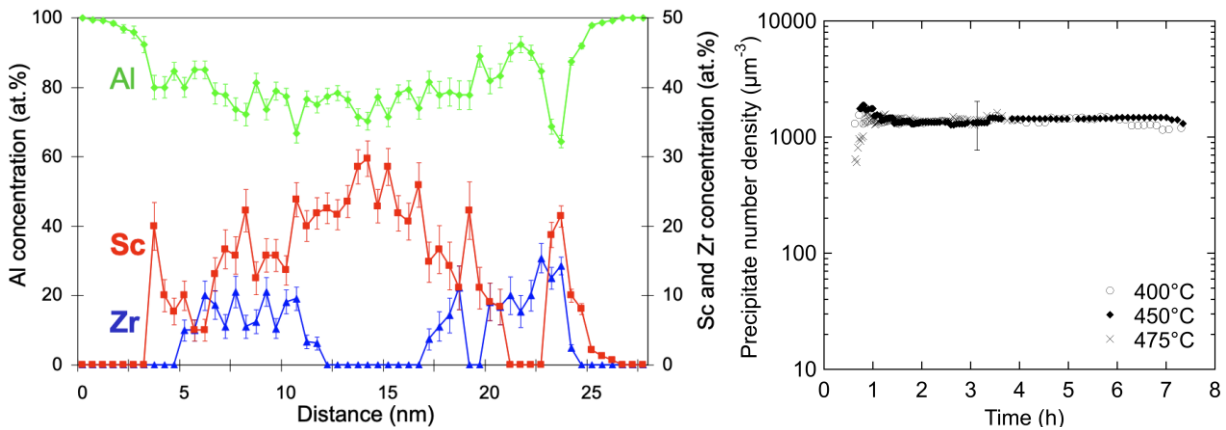


Figure 8: Left : solute distribution across an $Al_3(Zr,Sc)$ precipitate measured by APT, evidencing the core-shell structure with a Sc-rich core and Zr-rich shell (from [138]). Right : the Zr-rich shell

prevents precipitate coarsening, resulting in a constant precipitate number density with time as evidenced by in-situ SAXS (from [136]).

A similar situation exists in multicomponent steels where the diffusivities of the interstitial C and substitutional solutes differ by a factor of $\sim 10^6$. The precipitation of cementite during the tempering of multi-component martensite (e.g. Fe-C-Mn) first occurs with a substitutional composition corresponding to the bulk alloy composition of the substitutional lattice. As precipitation proceeds, the partitioning substitutional element content (e.g. Mn) gradually increases to the equilibrium value, which can be as high as 40 or 50% for Mn [101,102]. These deviations from stoichiometry are kinetically driven and are frequently observed.

Non-stoichiometry evolution of precipitate chemistry can also be driven by complex diffusion mechanisms involving cross-terms in the Onsager diffusion matrix, resulting in coupling of diffusion fluxes during diffusion. Such mechanisms have been extensively described during precipitation of γ' in multi-component Ni-based alloys [114,139,140].

Modelling the evolution of the precipitate composition during the course of precipitation has generally been made in the (relatively) simple case of a uniform precipitate composition. It involves finding at each time step the optimal compromise between thermodynamics and kinetics to optimize the precipitate growth rate. However, precipitation frameworks that properly treat multicomponent diffusion are capable of describing evolutions in the compositions inherited by the precipitate at the interface as a result of changes in the operative interfacial tie-lines. Examples include commercial codes such as TCPRISMA or the the Svoboda-Fischer-Fratzl-Kozeschnik (SFFK) model, based on the Onsager extremum principle [141]. The applications to non-stoichiometric precipitate evolution prediction, compared to experimental data, is widespread [124,142–150]. A subtlety, is to properly describe the evolution of the precipitate composition under conditions where the significant deviations in chemistry that are observed during precipitation do require one to self-consistently describe diffusion both in the matrix and in the precipitate. Most precipitation models do not currently capture the latter. A practical example where the latter is required is shown in refs [101,102].

7.3. Interface segregation

In addition to the effects discussed above, large deviations to the precipitate composition can be observed at the precipitate / matrix interface due to segregation or anti-segregation effects. These deviations can help decrease the cost of these interfaces through the combination of lower chemical and structural contributions, and/or decreasing the lattice strains between the two phases. Kinetics effects such as those presented for core-shell precipitates in the preceding sections may also be present. Reducing the interfacial energy can help the nucleation process [151] and when slow diffusing species are present at the precipitate interfaces, strain fields are reduced and/or the interfacial energy is reduced, the coarsening resistance can be enhanced [152]. Many systems exhibit solute segregation at the precipitate-matrix interfaces with resulting combinations of these effects, such as in Al-Cu [153–158], Al-Cu-Li [19,159], Al-Cu-Ag [160,161], Al-Zn-Mg [162,163], Al-Mg-Si-Cu [164], Al-Ni-Zr [165], Mg alloys [166,167], precipitates in steels [168,169], or superalloys [170–173].

8. Non-spherical precipitates

In most practical cases, the precipitates in metallic alloys are non-spherical. This is to be expected when two crystals of different structure are in contact, since the different interface

planes do not have the same energy and mobility. The non-spherical shape of the precipitates arise from the combination of at least three factors: anisotropy of interfacial energy, anisotropy of growth rate (including anisotropy of the interface mobility), and anisotropy of elastic energy (coherency strains). A fourth factor, which is related to heterogeneous nucleation sites, will be discussed in section 10. It is not the purpose here to review in detail the different mechanisms leading to anisotropic shapes, but rather to show how these shapes influence the precipitation kinetics, and how this can be described by modelling.

One can separate the cases of non-spherical particles into moderately anisotropic and highly anisotropic. The first category applies when the distance between precipitates is much larger than their maximum dimension, this condition becoming more restrictive as the precipitate volume fraction increases. In this first case, one can expect the diffusion field around a precipitate to be of nearly spherical symmetry at a certain distance from the precipitate, and thus the diffusion-controlled precipitation kinetics from spherical precipitates can be applied with reasonably good confidence, by simply calculating an equivalent precipitate size. Such models have been applied also in cases where these hypothesis were not necessarily met, for the sake of simplicity [174].

In all other cases, the situation becomes much more complicated, as the anisotropic diffusion fields of the growing (or shrinking) precipitates interfere in complex ways. Precipitates may experience soft impingement of their diffusion fields [175], or even hard impingement with precipitates meeting each other [176], long before the equilibrium volume fraction is reached, thus allowing precipitation to occur in several stages and leading to extreme overlap of growth and coarsening regimes of precipitation [177].

A classic example is the precipitation of plate shaped precipitates in Aluminum alloys (Fig. 9). In these cases, the aspect ratios of the plates exceed 10 and soft impingement of the diffusion fields at the tips of the plates occurs long before most solute has been removed from solid solution.

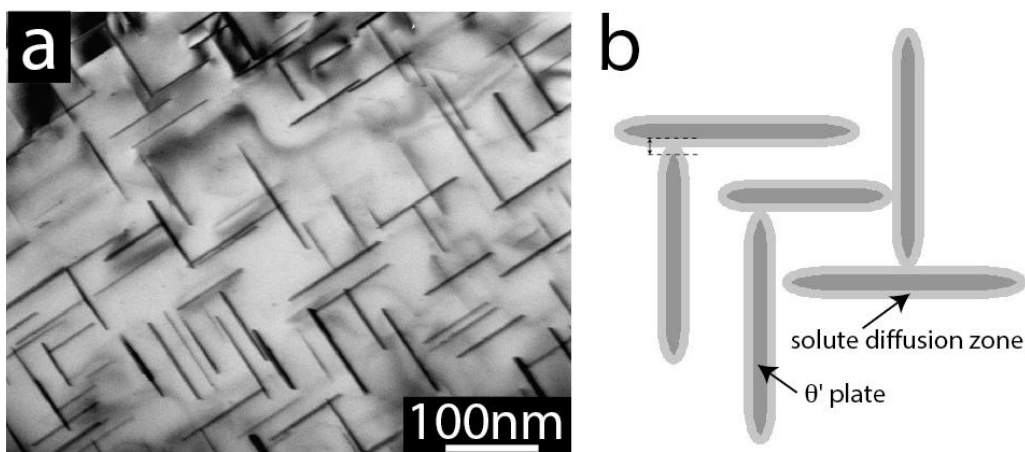


Figure 9: a) Bright field TEM micrograph showing plate-shaped θ' particles formed in an Al-Cu alloy after aging for 4h at 200°C, b) a schematic illustration of the anisotropic solute diffusion fields that accompany plate shaped particles showing that soft impingement at the plate tips occurs long before all of the solute is removed from solution. In the Al-Cu case, the peak aged state at 200°C corresponds to 4h ageing and only ~ 50% of the solute supersaturation has been relieved at this time (modified from [175]).

Experimentally, the evolution of the different characteristic dimensions of the precipitates can be obtained from the analysis of non-isotropic SAXS patterns when the main precipitate axes

are aligned with the incoming X-ray beam [178,179]. Some misalignment can be dealt with by appropriate calculations. This, coupled with in-situ measurements during heat treatments, makes it possible to evaluate the independent evolution of the different precipitate dimensions during the course of precipitation [180,181]. An example of the evolution of the length (diameter) and thickness of T_1 (Al_2CuLi) precipitates during ageing of an Al-Cu-Li alloy is shown in Fig. 10.

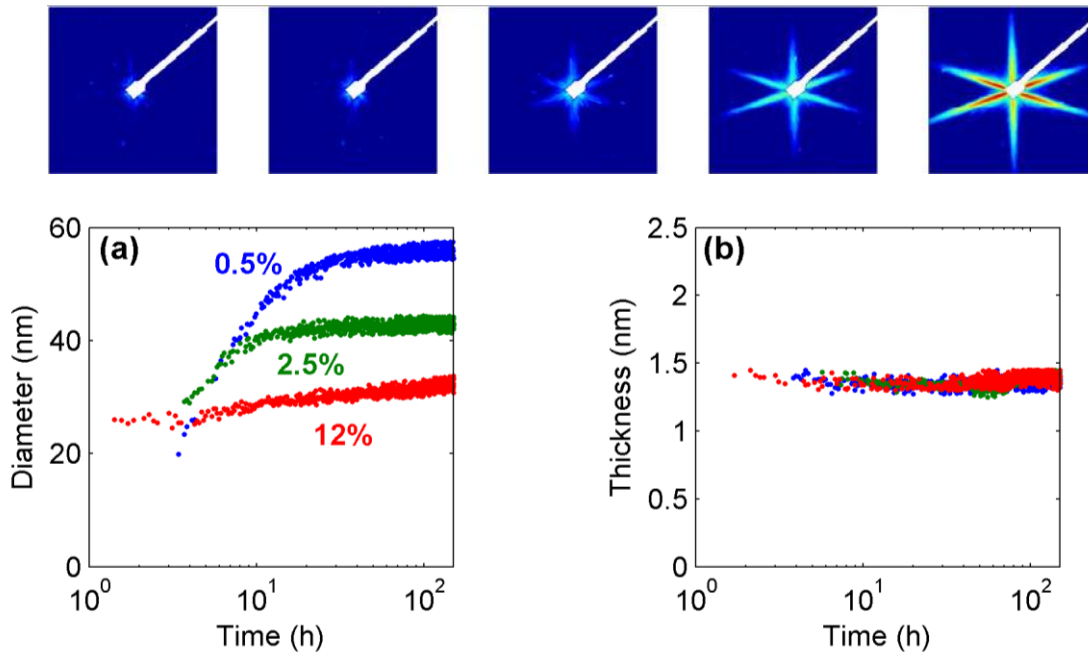


Figure 10: Top: Evolution of SAXS patterns during ageing at 155°C of an Al-Cu-Li alloy, showing the development of streaks whose shape is characteristic of the high aspect ratio T_1 precipitates. Bottom: from these images the thickness and diameter of the precipitate plates is calculated, allowing to evidence the effect of pre-deformation on the precipitation kinetics and aspect ratio evolution (from [180]).

Precipitation kinetics models for anisotropic particles require some knowledge of the shape evolution during the course of the phase transformation. Depending on the crystallography of the precipitate / matrix interface and on the growth mechanism, several different hypotheses can be made to calculate the evolution rate.

Prior to soft impingement, the lengthening rate of needles or plates is relatively constant and can be described by the Zener-Hillert equation (Eq. 4) [73]. This description has been used, in combination with the prediction of soft impingement by the consideration of the extension of the diffusion field, to describe the lengthening of precipitate plates in Aluminum alloys, Fig. 9 [175], and Magnesium alloys [182].

The equilibrium shape can be computed using both interfacial energy and elasticity, leading to the prediction of the precipitation of anisotropic precipitates [183,184]. These simulations show that this equilibrium assumption overlooks the effect of growth mechanisms (and their effects on the interfacial mobility) and thus deviates from experimental observations. Realistic shapes can be computed by phase field modelling when introducing all aspects of interfacial anisotropy and elastic strains [185], see Figure 11. Another possibility is to use the thermodynamic extremal principle to predict the evolution of the aspect ratio from the anisotropy of strain energy [186].

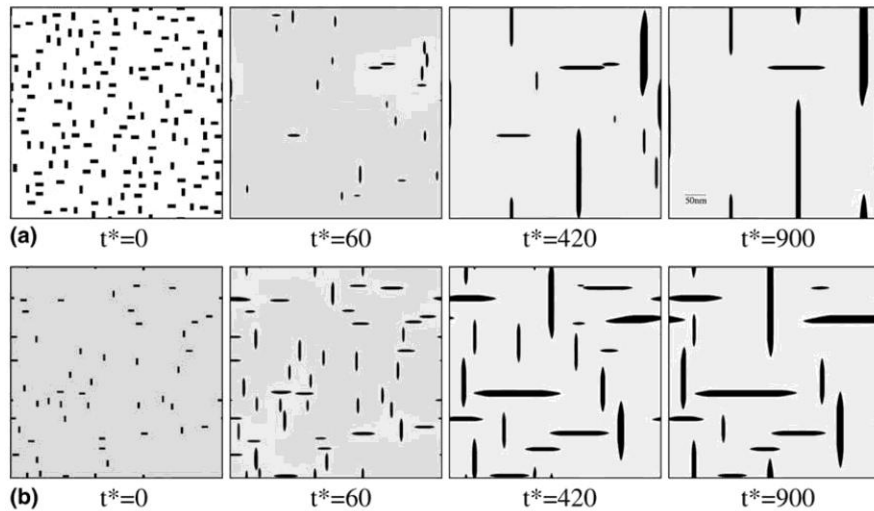


Figure 11: Prediction of precipitate evolution during precipitation in Al-Cu by a multi-scale phase field approach (from [185]).

Another possible assumption is to consider a constant aspect ratio, which could correspond to an equilibrium Wulff construction, balancing the anisotropy of interface energies. In this case, models have been proposed as a simple evolution of the spherical KWN models, such as in a 6xxx series Aluminum alloy where the lengthening rate of needle-shape precipitates was calculated from the Zener-Hillert equation [187], or in the 718 Ni-based superalloy [188], and implemented in a class precipitation model. More advanced corrections to the growth rate of non-spherical precipitates have been developed [189] and implemented in KWN-type models, with the ability to predict the evolution of the aspect ratio together with that of the precipitate size distribution [190].

The thickening rate of plate-shaped particles with well-defined planar interfaces shows a very different kinetics from its lengthening, as it can be controlled by a separate mechanism of ledge nucleation [191]. This is very system dependent, and explains why in some cases precipitates can lengthen at constant thickness if thermal activation does not allow thickening to occur and thicken at higher temperature [46,176,180], or grow at relatively constant aspect ratio, yet with a different rate constant as for traditional growth / coarsening [192].

9. Multi-phase precipitation, metastability trajectories

Multiple phases can precipitate together due to two factors: due to an increasing number of solute species in the alloy which increases the number of phases that can coexist at equilibrium, and, more generally, due to the existence of metastable phases, favored kinetically over the stable phases. Even in modestly complex alloys, e.g. Al-Mg-Si-Cu, one can find up to half a dozen different phases together at a given time, and they evolve in a complex manner towards a more stable state [11]. One should emphasize that in most cases, the metallurgical states of interest for practical use precisely contain these metastable phases, which are usually dispersed at a finer scale than the stable ones.

Understanding how the material follows a sequence of phases during the course of a phase transformation is one of the most classical problems in physical metallurgy. This sequence is sometimes called a “precipitation sequence” or a “metastability cascade”, however it is probably more appropriate to use the concept of “precipitation trajectory”, which emphasizes that this trajectory is not unique to a given system - it can depend sensitively on the exact chemical composition and on the thermal path followed.

When multiple precipitates form together and in sequence, it is not possible to describe their kinetics as if they were forming alone from a uniform solid solution. The simplest coupling between the different phases occurs by only considering the effect of the average solid solution content. In this case, the formation of the most stable phase is made possible because the solubility of the matrix in equilibrium with the metastable phase is higher than that of the stable phase. Since the metastable phase is favored kinetically (or else it would not be observed), it forms first, and is later destabilized by the formation of the stable phase which takes over with time. Such a simple coupling is able, for instance, to describe successfully the competition between precipitation of ϵ -carbides and cementite in low-carbon steels [193], Fig. 12.

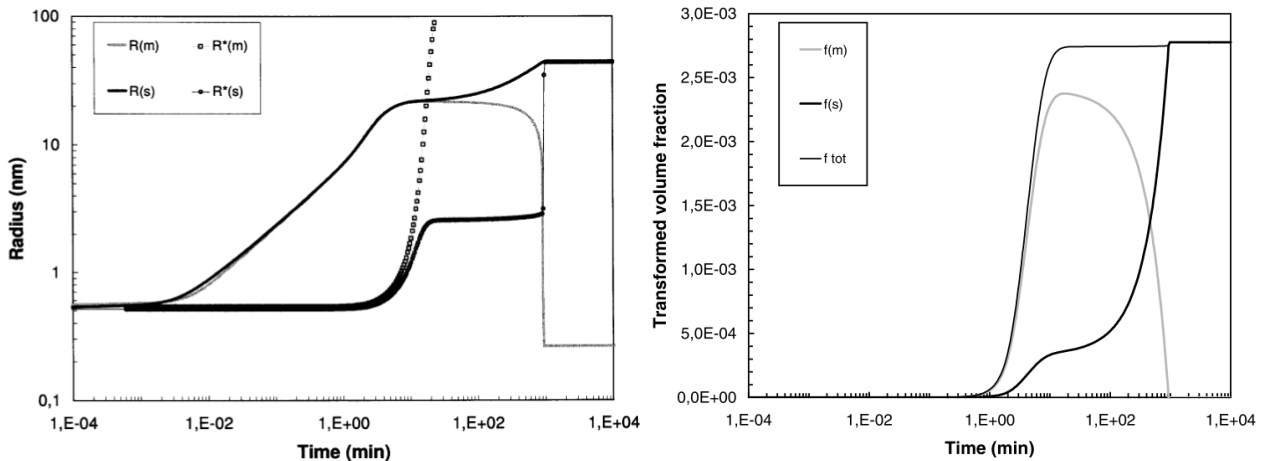


Figure 12: predicted competition between precipitation of ϵ -carbides (m for metastable) and cementite (s for stable) in a low-carbon steel at 200°C, with the radius and volume fraction evolution of both phases (from [193]).

This type of coupling has also been used to describe the evolution from clusters to precipitates in 6xxx series (Al-Mg-Si based) aluminum alloys [194]: the clusters that form during room temperature ageing reduce the solute content and thus usually make the formation of the next phase (β'') more difficult [195]. This coupling through the solid solution has been implemented in commercial software such as Matcalc where it has been used to describe the sequence of phases in 6xxx series Aluminum alloys [196] or in TC Prisma where it has been used to describe the competition between different carbides in steels [65] or the transition from clusters to S phase in 2xxx series Al-Cu-Mg [43]. These examples require a suitable description of the Gibbs energy of the clusters as a function of composition and temperature which brings us back to the question of what defines a precipitate discussed in section 3.

A second mechanism for multi-phase precipitation is the in-situ transformation of one phase into another. We have seen in the previous section that in the general case gradual composition changes occur during precipitation within a given crystallographic structure; these changes can trigger a structural transformation when reaching a critical value. Another parameter that may affect the precipitation kinetics is a loss of precipitate coherency, which usually is predicted to happen above a critical size, and results in a change of interfacial energy, translating into a change of Gibbs-Thomson effect and thus a change of interfacial matrix concentrations.

The internal crystal structure of the precipitate can also change (gradually or abruptly) during precipitation. A classic example is the precipitation of Cu in Fe. During early precipitation

stages, Cu precipitates have the BCC structure of Fe, and they progressively transform into an FCC structure through complex internal transformations involving multi-twinned structures. The description of the transition between these structures is obviously complex, but was first simplified to a criterion on precipitate size [197], before recent phase-field modelling has been able to describe the occurrence of the internal displacive transformation [198]. Another classic case is the evolution of GPI zones in Al-Cu alloys (a single atomic plane of Cu) into GPII zones (two atomic planes), which simply requires adding atoms to the initial structure, followed by more abrupt changes in structure towards the θ' [199] and θ phases [55]. An interesting case of this in-situ transformation is when the metastable state contains some crystallographic building blocks of the precipitate which will form from it. In the Al-Mg-Si system, for instance, it has been shown that some specific cluster states contain atomic arrangements similar to those encountered in the β'' phase, which has been interpreted as facilitating the formation of the latter phase during subsequent ageing [200]. The obvious advantage of this internal structure is that the transition to the stable phase does not require any nucleation, so that it can happen with almost no barrier. In terms of the kinetics of such a transition, one should distinguish cases where the composition of the metastable phase and the more stable phase that it replaces are equal (e.g. Cu precipitates in Fe), with cases where there is a change of composition. In the first case, once the criterion for the transition is reached, the transformation can be expected to be almost instantaneous. In the second case, the change of composition requires transport of solute by diffusion, which controls the transition [201].

The last mechanism by which it is possible to couple several precipitates forming together is heterogeneous precipitation of a new phase on the existing one. The new phase may take advantage of the particular crystallographic arrangement at the interface between the first phase and the matrix, or simply of the presence of an interfacial energy and a reserve of solute. In this case, the heterogeneous nucleation of the new phase should be thermally activated, and once it is nucleated the new phase can grow very rapidly by destabilizing its neighbor and incorporating its solute. If a large change of composition is involved, some more long-range diffusion of the missing species may be necessary. Examples of such transitions include the transition between different S phases in Al-Cu-Mg [39,43], or the complex multi-phase structures found in Al-Cu-Li-Mg alloys, where T_1 , Al-Cu GP zones, θ' and S precipitates are observed to be all connected to each other [19,159], as shown in Fig. 13.

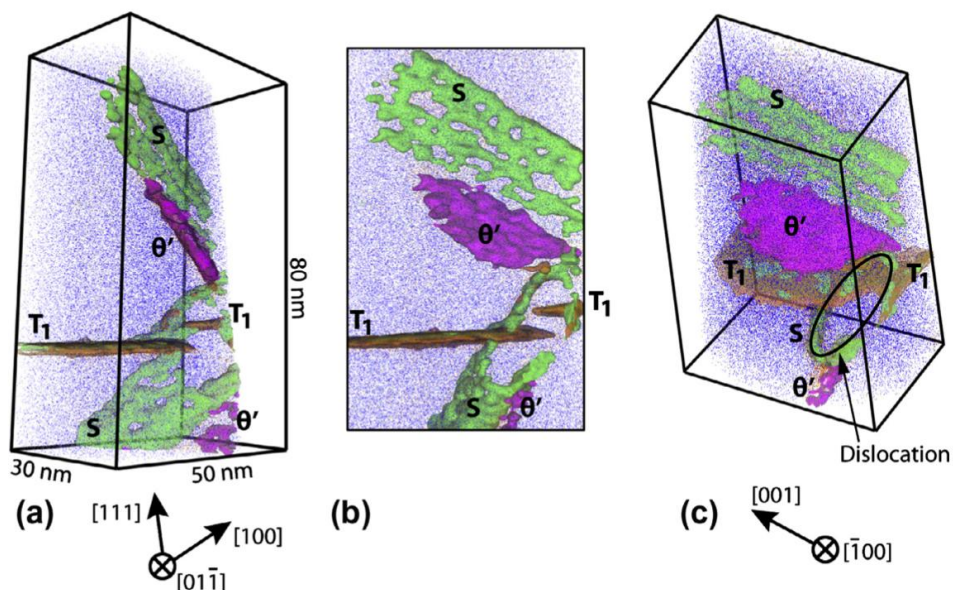


Figure 13: APT volume reconstruction of an aged Al-Cu-Li-Mg alloy showing the presence of multiple phases connected to each other: T_1 (Al_2CuLi), θ' (Al_2Cu) and S (Al_2CuMg) (from [19]).

Many other examples exist of structural transformations of precipitates, e.g. Ni-Al based precipitates in Fe alloys [202], transition from spinodal decomposition to G-phase precipitation in steels [203], complex precipitation sequences in Mg alloys [204,205], co-precipitation of γ'' and γ' in Ni based superalloys [206].

10. Heterogeneous precipitation on structural defects

Except for systems where precipitation occurs with a high driving force and a very low interfacial energy, homogeneous nucleation in metallic alloys is generally impossible. It is more common for nucleation of phases to occur by a sequence of metastable phases, as seen in the previous section, and/or by heterogeneous precipitation on structural defects such as dislocations and grain boundaries. When the precipitation kinetics is compared between materials with large differences in defect density, many effects that will be detailed below are coupled, and result in a change of the nature and scale of precipitation. When a material is plastically deformed prior to a precipitation ageing treatment, the presence of a high dislocation density frequently changes the precipitation sequence towards equilibrium phases that are difficult to form otherwise and accelerates the precipitation kinetics [207,180,208–212]. In materials with very small grain sizes, such as achieved by severe plastic deformation, the precipitation kinetics can be shifted to much lower temperature [213] and in extreme cases coarse precipitates characteristic of high temperature precipitation can be found after room temperature storage [214].

At least four factors need to be considered to account for heterogeneous nucleation and to understand its kinetics:

- The presence of a pre-existing excess energy, essentially an interfacial energy for grain boundaries, and an elastic energy for dislocations. This pre-existing excess energy favors nucleation by biasing the energy balance and decreasing the energy barrier, in the case where there is at least a partial wetting tendency of the precipitate on the structural defect.
- The crystallographic matching between the precipitate and matrix may be more favorable than for homogeneous nucleation, and nucleation on defects may favor some phases and/or special orientation relationships [215]. For instance, when forming a hexagonal precipitate in an FCC matrix, the presence of a dissociated dislocation provides the necessary stacking fault that allows a coherent matching on the dense packed planes [216].
- The crystal defects interact not only with precipitates, but also with solutes. Prior to nucleation of the precipitates, there is usually a tendency for solute segregation at the crystal defect [217]. This solute segregation changes the solute distribution and thus influences nucleation [218–220]. It provides a solute distribution which should facilitate nucleation, but on the other hand the presence of segregation modifies the energy of the crystal defect and thus may decrease the first effect described above.
- The presence of a crystal defect changes the solute diffusion kinetics, both quantitatively (dislocations and grain boundaries are fast diffusion paths) and qualitatively (the geometry of diffusion is modified and thus the spatial distribution of solute) [221]. If the crystal defect moves during precipitation, it can act as a solute collector plate and further accelerate the kinetics [214,222].

Taking all these effects into account, it is generally observed that nucleation at structural defects occurs faster than homogeneous nucleation. In some cases, only heterogeneous precipitation is ever observed [223,224]. A common feature is also that heterogeneous

precipitation favors the formation of more stable phases [225] (which could not have formed homogeneously), so that a mixture between stable phases at structural defects and metastable phases in the matrix may be observed [195].

To describe nucleation at structural defects, the CNT equation might be modified so long as the nucleation barrier can be calculated with sufficient precision, the kinetic pre-factor can be modified to reflect changes to the diffusion geometry and that one takes into account the effective number of nucleation sites available for nucleation [226]. This is by no means straightforward. It is doubtful that a stationary nucleation rate applies for very long during heterogeneous nucleation. Once the initial solute at the defect is used for the first nuclei, nucleation of new particles rely on solute diffusing from the bulk towards the defect. A solute reaching the defect can diffuse rapidly along it to an existing precipitate, or be used to form a new one. The probability of further nucleation depends on the competition between these two mechanisms. This effect has been successfully implemented for describing the nucleation at dislocations of NbC in Fe [227].

After nucleation is complete, the growth and coarsening rates at structural defects have very different characteristics from those of homogeneous precipitates. Two cases need to be considered:

- Firstly, the case where the heterogeneous precipitates are alone in the microstructure, for instance the precipitation of NbC in a Fe alloy containing a sufficient density of dislocations, see Fig. 14. The kinetics of growth and coarsening is then completely determined by the geometry of solute diffusion. When solute transport occurs only by diffusion along the crystal defect, coarsening rates as $t^{1/4}$ and $t^{1/5}$ have been predicted by theory for grain boundaries and dislocations [228,229], respectively. An interesting effect in such a case arises from the geometry: since the precipitates are in contact only via the crystal defect, there must be much stronger correlation between neighboring precipitates, even in dilute systems. In practice, it is necessary to account for both fast diffusion pathways and volume diffusion, and derive appropriate models to describe the precipitate evolution in such mixed diffusion geometry [228,230].

- The second case is when precipitation at structural defects is competing with homogeneous precipitation. A classic case is the development of precipitate-free zones on each side of grain boundaries in precipitate containing Aluminum alloys, which has a strong effect on fracture, fatigue and corrosion properties. Similar precipitate-free zones can develop around dislocations for the same reasons, and in the presence of dislocations, homogeneous and dislocation-based precipitates can form competitively such as in direct-aged 718 Ni based alloy [231]. Although the presence of these PFZs is not only determined by solute fluxes (vacancies annihilated at the structural defect play a prominent role), the evolution of the precipitate microstructure is in this case determined by the neighborhood of two different precipitate families, at the grain boundaries and in the bulk. Usually, precipitates at the structural defect are both more stable (stable vs. metastable in the bulk, see above) and larger (due to faster diffusion at the defect). These two features add and result in a solute concentration gradient in the matrix towards the defect, which tends to dissolve the homogeneous precipitates lying closest to the PFZ, increase the size and volume fraction of the heterogeneous precipitates and increase the size of the PFZ with time, see Fig. 15 [69,222].

Taking all effects globally into account in an integrated model remains challenging. However it has been achieved with some simplified assumptions in a number of cases [195,222,227,232].

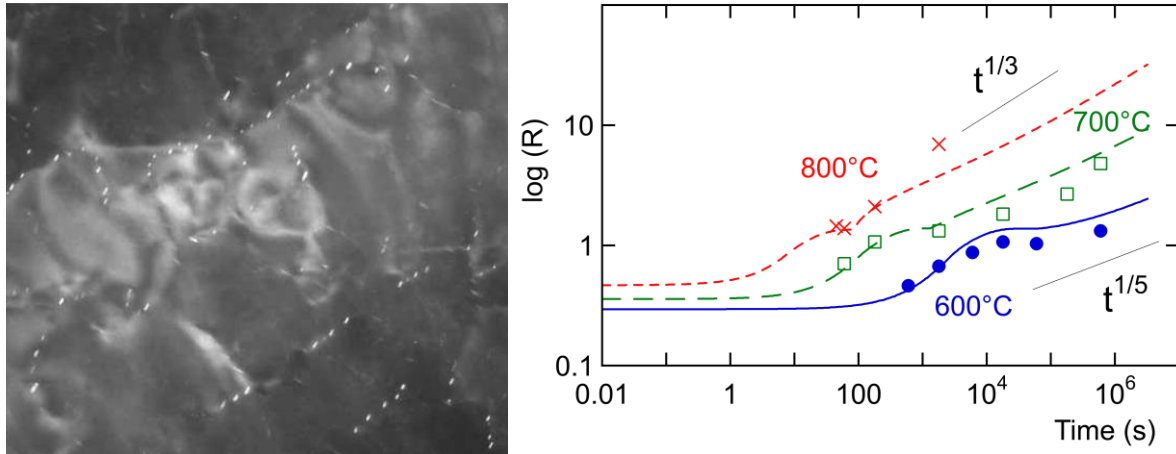


Figure 14: Left: dark field electron micrograph showing NbC precipitates in Fe solely forming at dislocations (adapted from [223]). Right: Predicted kinetics of heterogeneous precipitation at different temperatures compared to SANS results, showing the transition from bulk diffusion control ($1/3$ time exponent) to pipe diffusion control ($1/5$ time exponent) as temperature is decreased (adapted from [227]).

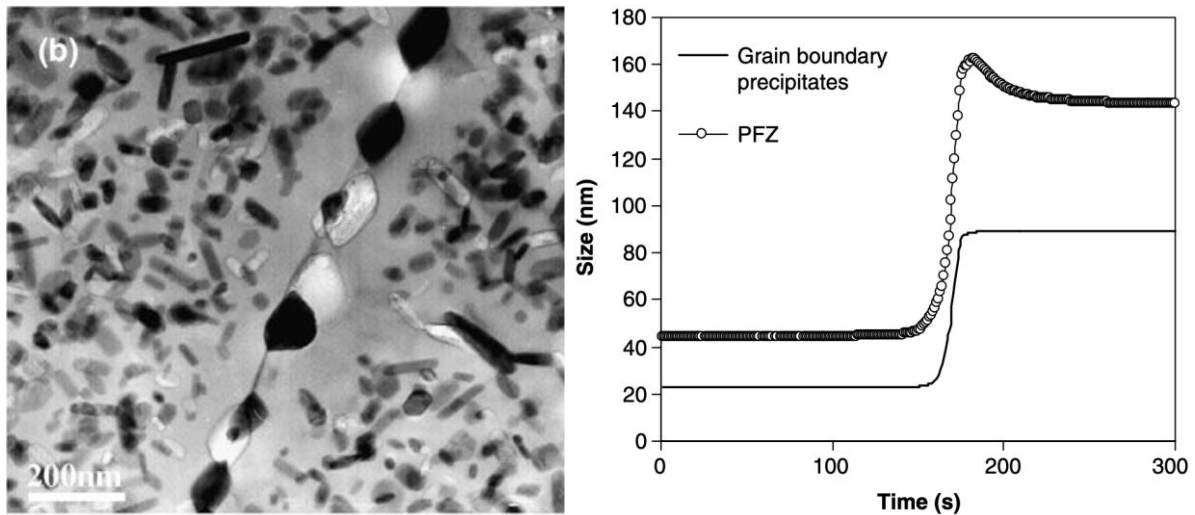


Figure 15: Left : Large grain boundary precipitates surrounded by a precipitate-free zone in a friction stir welded Al-Zn-Mg-Cu alloy ; right : predicted evolution of the size of grain boundary precipitates and of the PFZ during the welding cycle (from [222]).

Finally, strong coupling can occur between the movement of crystal defects and precipitation, when these occur concurrently, so-called dynamic precipitation is observed (e.g. [31,233–236]). This coupling results in a very wide variety of kinetic effects, which will not be detailed in this review.

11. Non-isothermal effects

Precipitation is generally studied along isothermal paths, which ensures stable thermodynamic conditions and simplifies the description. However, in many practical situations, precipitation occurs non-isothermally. This is the case when a part of large thickness is quenched from the solution treatment temperature, and when precipitation occurs during cooling to room temperature. Conversely, in many cases heating towards a precipitation heat treatment temperature occurs at a finite rate, either intentionally or

incidentally because of the material's large dimensions. During specific secondary heat treatments, among which welding is the archetype, a temperature spike can occur which profoundly modifies the precipitate microstructure.

During these temperature changes, all physical parameters that control the precipitation reaction change, especially the solubility within the parent phase, the driving force for precipitation and the diffusion rate. Non-equilibrium effects such as the capillarity effect (Gibbs Thomson effect) experience changes in magnitude, as well as the surface energy. Therefore, the precipitation kinetics may show a variety of specific features due to the non-isothermal nature of the ageing path.

To describe the variety of specific features (as compared to isothermal precipitation) that can be found, we will follow the different stages of a classical precipitation treatment: quench-induced precipitation, precipitation during non-isothermal heat treatments, and finally the effect of secondary processes (welding).

An ideal quench from the solution treatment temperature should leave the solid solution in a supersaturated state. Even when the quench is made very rapidly, a detailed analysis of the solid solution shows generally some deviation from a random solid solution (which is not homogenous and would anyway contain clusters!). It is recognized that the exact quench conditions (solution treatment temperature and quench rate) can have large consequences on the subsequent phase transformation kinetics, as has been evidenced for spinodal decomposition in Fe-Cr alloys for instance [237,238]. In many practical applications, it is either not possible to perform an ideal quench due to the size of the parts to be quenched, or not desirable because an ideal quench would lead to unacceptable levels of internal stresses. In this case, precipitation can occur during quenching (autotempering of martensite is an example). Particularly in Aluminum alloys, large efforts have been made to characterize in detail the kinetics of this non-isothermal precipitation upon cooling, particularly using combinations of calorimetry techniques [50], and to model its kinetics [239,240]. Since temperature is decreasing, all phenomena occurring at high temperature can be considered to be 'frozen' at lower temperature, where other phenomena can take place. Thus, precipitation at high temperature consists mostly of heterogeneous precipitation at structural defects or insoluble phases, which is followed by formation of metastable phases, GP zones or clusters during the late stages of cooling at lower temperatures [241,242]. The kinetics of these processes is in principle relatively easy to describe from those of isothermal experiments. Once a precipitate nucleates, since the temperature continuously decreases, its thermodynamic stability continuously increases and thus it will continuously grow with an increasing solute contrast within the matrix between the concentration at the interface and the residual matrix concentration. Coarsening is unlikely (except for very slow cooling rates) and destabilization cannot happen. In Ni based superalloys, precipitation during cooling of the γ' phase (either during multi-step isothermal treatments or during continuous cooling) is classically used and results in multi-modal precipitate distributions [243,244].

However, one complexity can arise due to the behavior of vacancies, which become supersaturated during cooling and therefore experience their own kinetics of annihilation at the structural defects of the microstructure (grain boundaries and dislocations). Depending on this annihilation kinetics relative to the precipitation kinetics, the two can become strongly coupled. As an example, in-situ SAXS study of quench-induced precipitation in a 7xxx series Aluminum alloy has shown that the kinetics of GP zone formation during the late stages of quenching did not depend on quenching rate, because the smaller time left for precipitation during fast quenching was compensated by a larger retention of quenched-in vacancies [104], Fig. 16.

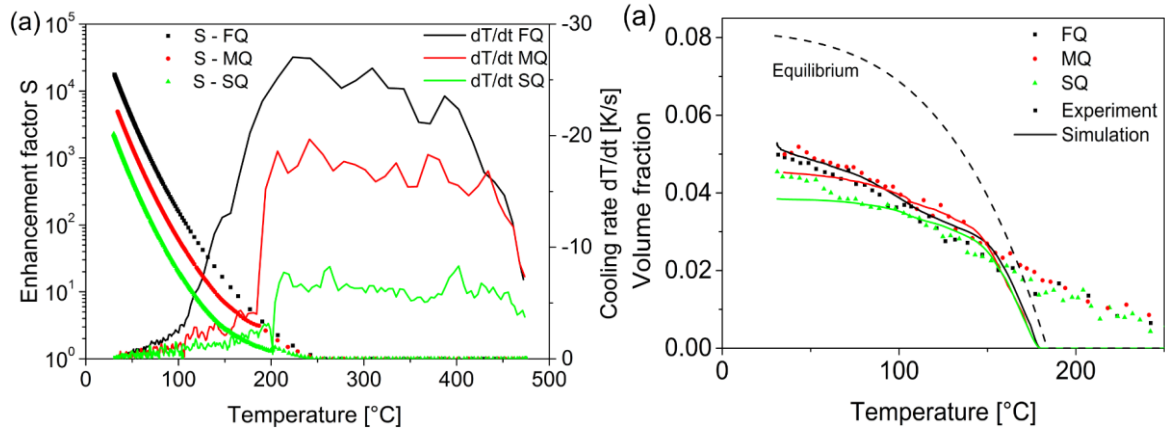


Figure 16: Left: Calculated evolution during three cooling schedules (fast, medium, slow) of the vacancy supersaturation with temperature in an Al-Zn-Mg-Cu alloy quenched from the solutionizing temperature. Right : Volume fraction of precipitates formed during quenching measured by in-situ SAXS, compared with modelling, showing the compensation between diffusion time and vacancy concentration in controlling the precipitation kinetics (from [104]).

A second point which needs to be carefully accounted for, especially when considering subsequent precipitation during ageing, is the geometry of the solute distribution at the end of quenching. A good example is the effect of coarse quench-induced heterogeneous precipitation on subsequent nanoscale precipitation during ageing. Most models describing this effect consider that precipitation during quenching uniformly decreases the solute available for subsequent precipitation [245]. In fact, the solute distribution after quenching is very heterogeneous, with a strong depletion around quench-induced precipitates, resulting in the formation of a precipitate-free zone, whereas the remaining material behaves similarly to a perfectly quenched material [246]. Quench factor analysis (e.g. [247]) describes the resulting strength as a fraction of the strength obtained after an ideal quench, thus making an assumption of a simple law of mixtures between unaffected material and soft, nanoscale precipitate-free material.

The second situation where non-isothermal effects are important happens when ageing is carried out using non-isothermal routes. In most industrial situations, the heating of parts to the ageing temperature can take several hours, which renders ageing non-isothermal by necessity [30,248]. In some cases, the ageing treatments are purposely non-isothermal or multi-stage, usually with increasing temperature (like the two-stage classical ageing of 7xxx series Aluminum alloys [246]) or more complex (like the retrogression and re-ageing treatment of the same alloys [130] or two stage ageing to promote bi-modal precipitate distributions [249]). At the extreme of this logic, non-isothermal ageing treatments can be designed *ad hoc* to either optimize a final microstructure, minimize the time of the heat treatment, minimize the energy consumed, etc., such as been demonstrated with the Fe-Cu system [250], see Fig. 17.

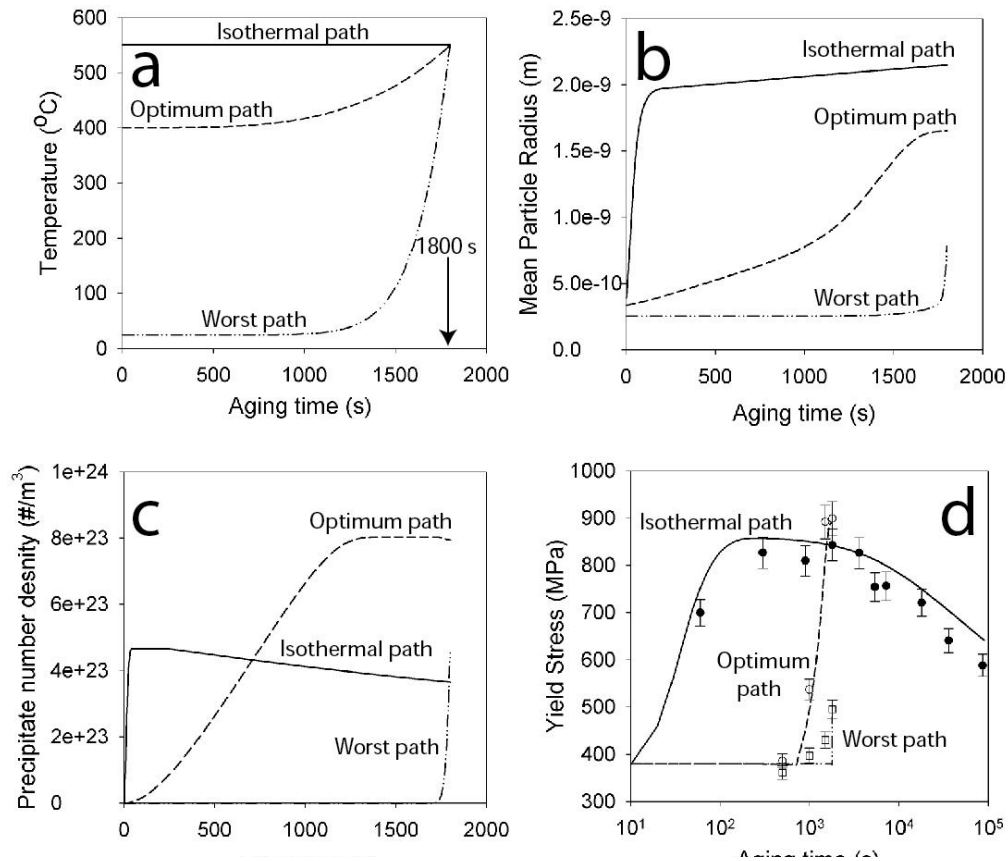


Figure 17: Result of designing an optimal non-isothermal heat treatment path for precipitation in an Fe-Cu alloy, showing that it is possible when compared to isothermal precipitation to reach a higher number density and lower precipitate size, and a higher resulting strength (from [250]).

Designing a multi-stage heat treatment can follow two purposes: decouple nucleation and growth, and take advantage of metastable-to-stable phase transitions. In both cases, the rationale is that at low temperatures nucleation is favored by the high supersaturation and / or by the possibility to form metastable phases of low interfacial energy. Once low-temperature nuclei are formed, their growth may be extremely slow, and in the case of metastable phases such as GP zones they may not provide the appropriate properties, such as strengthening, as compared to precipitates further along the precipitation trajectory. This leads one to increase the temperature to promote diffusion and/or transition to more stable phases. An important point to monitor is the evolution of the nuclei formed at low temperature during heating. When temperature is increased, the stability of these nuclei decreases, and it is often observed that they start to dissolve, at least temporarily, before transition to a more stable phase or irreversible growth takes place [37,251]. If the extension of this dissolution is too large, the influence of the low-temperature nucleation stage becomes ineffective. As an example, it has been shown that applying a fast heating rate during artificial ageing of a naturally aged 7xxx series Aluminum alloy has a negative effect on the nucleation of the strengthening η' phase due to the dissolution of the GP zones, as compared to a slower heating rate [252]. On the contrary, when low-temperature phases do not serve as nuclei for the strengthening phase, such as in Al-Mg-Si alloys, one can aim to minimize the time between quench and ageing and minimize the heating ramp to retain the solid solution for efficient nucleation. Alternatively, in this system, even more complicated non-isothermal heat treatments have been designed with pre-ageing heat treatments between quench and artificial ageing, which favor the formation of “good” clusters which can efficiently transition to the strengthening phase [253,254].

The third case involves situations where an existing precipitation microstructure is subjected to a strongly non-isothermal heat treatment, resulting in changes of the precipitate characteristics. This happens obviously during classical welding, where the heat-affected zones are subjected to a temperature spike (we will not discuss here what happens in the fusion zone), during solid state welding (e.g. friction stir welding), where these temperature spikes can be accompanied by substantial plastic deformation, and other processes, such as laser surface treatments [255] or additive manufacturing [256]. The common feature is a precipitate microstructure subjected to a temperature spike, which includes a temperature increase, followed by a temperature decrease. What happens to the latter corresponds to what happens during quenching, with the difference that the microstructure at the maximum of temperature is generally far from a homogeneous solid solution (except for very high peak temperatures). Thus, we will concentrate on what happens during heating, usually called *reversion*, illustrated by modelling results in Fig. 18. When temperature is increased, the stability of the precipitates decreases. This translates into an increase of the critical radius for dissolution R^* , which becomes at one point larger than the radius of existing precipitates, triggering their dissolution [257]. Since this dissolution occurs concurrently to the growth of the largest precipitates (which may still be larger than R^*), it is often observed that during the early stages of reversion the volume fraction of precipitates decreases but the average radius remains constant [258,259]. When dissolution proceeds, two cases can be encountered: either the precipitates become less and less stable, then the precipitates finish to dissolve, their size decreases, ending with a full solid solution; either the increasing level of solid solution resulting from partial dissolution stabilizes the remaining precipitates (translating in a decreasing R^*), and the surviving precipitates can experience coarsening. Such multi-stage dissolution kinetics has been observed experimentally and described by modelling [257,260]. It explains the variety of microstructural states observed in weld heat-affected zones [261] or after laser surface treatments [255] depending on the heating and cooling rates experienced.

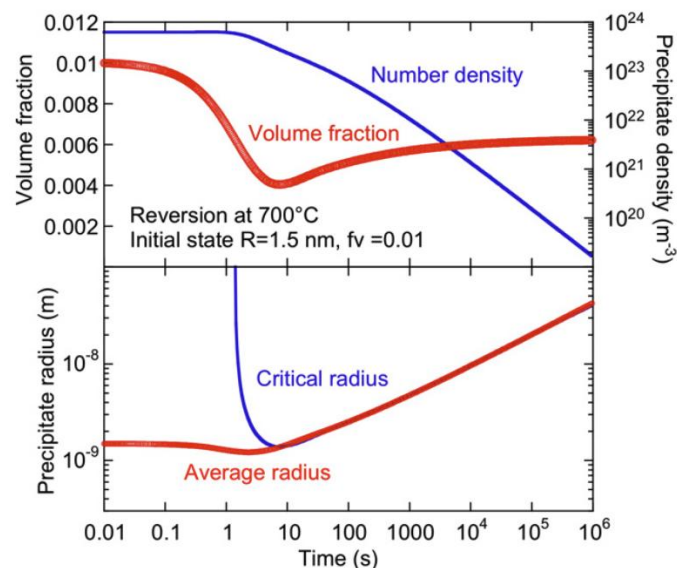


Figure 18: modelled evolution of precipitate size, number density and volume fraction, during a reversion heat treatment (from [259]).

Concluding Remarks

We have reviewed in this paper a number of issues raised by the understanding and quantitative description of precipitation kinetics in metallic alloys. As a conclusion, we have

formulated summary remarks about what we feel are important directions for future work in this area:

- Characterization and modelling tools have come so far in the last 10-20 years that many can now be used routinely, and the convergence between experiments and models has become widespread. However, work is still needed to develop a common data analysis framework to reach an unambiguous comparison of the two, especially when approaching the atomic scale.
- A quantitative description of nucleation that can be used generally in metallic alloys remains an issue. CNT, in the most commonly used form, is not applicable to solid state precipitation where there is a change in chemistry. It is used, but it is semi-quantitative at best. Precipitation models always need to be 'tuned' because of the uncertainty in describing nucleation. This is what prevents precipitation kinetics models from being properly predictive and this remains one of the major outstanding problems in solid state phase transformations. This issue is particularly outstanding in "realistic" cases involving semi-coherent phases, heterogeneous nucleation or sequences of clustering and metastable phases.
- Better experimental methods to quantitatively monitor vacancy behavior are needed, so that these important effects can be properly integrated into models. The effects can be large but we are very much limited at the moment in the characterization. PALS is extremely useful but quantification and separating signals from different positrons traps is non-trivial.
- Commercial software, coupled with thermodynamic databases, are nowadays widely available for precipitation kinetics modelling. These make precipitation modelling easily accessible, and the development of thermodynamic data for metastable phases widens their applicability. Yet the underlying assumptions are much less well established and appreciated, as compared to equilibrium thermodynamics, and one should be careful to understand these assumptions to avoid using such software as a "black box".
- We have described in this overview how different levels of complexity in the precipitation process can be described and understood. Many of the additional ingredients have now received an appropriate modelling description, however an integration of several of these remains mostly out of reach. Much work is now needed to integrate several of these approaches, e.g. to describe precipitation of non-isotropic particles nucleated on structural defects, non-isothermal effects in concentrated alloys, etc.
- With the development of high throughput experimental approaches, as well as high throughput modelling tools, the amount of data available describing precipitation kinetics will certainly grow considerably in the next years, although this will come at the cost of the level of precision of the microstructure characterization (no direct imaging possible). In cases where the complexity of phenomena prevents a predictive traditional modelling approach, machine learning approaches may be useful to reach a practical description of microstructure evolution, find optimal processing paths and help alloy design. This may be an interesting alternative approach to the nucleation problem.
- Precipitation coupled to plastic deformation is a very wide topic involving many different competing effects. These have been hardly addressed in this overview for lack of space, and would benefit from a separate overview to summarize the large body of work that has been published in the last 10 years.

Acknowledgements

Dr. Frédéric De Geuser is thanked for stimulating discussions. This work has been partially supported by MIAI@Grenoble Alpes (ANR-19-P3IA-0003) and the Australian Research Council (ARC) ([DP210102714](https://doi.org/10.1016/j.mater.2016.163)).

References

- [1] D.L. McDowell, R.A. LeSar, The need for microstructure informatics in process-structure-property relations, *Mrs Bull.* 41 (2016) 587–593. <https://doi.org/10.1557/mrs.2016.163>.
- [2] G.B. Olson, C.J. Kuehmann, Materials genomics: From CALPHAD to flight, *Scr. Mater.* 70 (2014) 25–30. <https://doi.org/10.1016/j.scriptamat.2013.08.032>.
- [3] S.C. Wang, M.J. Starink, Precipitates and intermetallics phases in precipitation hardening Al-Cu-Mg-(Li) based alloys, *Int. Mater. Rev.* 50 (2005) 193–215.
- [4] D.J. Chakrabarti, D.E. Laughlin, Phase relations and precipitation in Al–Mg–Si alloys with Cu additions, *Prog. Mater. Sci.* 49 (2004) 389–410. [https://doi.org/10.1016/S0079-6425\(03\)00031-8](https://doi.org/10.1016/S0079-6425(03)00031-8).
- [5] A. Simar, Y. Bréchet, B. de Meester, A. Denquin, C. Gallais, T. Pardoën, Integrated modeling of friction stir welding of 6xxx series Al alloys: Process, microstructure and properties, *Prog. Mater. Sci.* 57 (2012) 95–183. <https://doi.org/10.1016/j.pmatsci.2011.05.003>.
- [6] C.R. Hutchinson, Modelling the kinetics of precipitation processing in Aluminium alloys, in: *Fundam. Alum. Metall. Prod. Process. Appl.* Ed. R Lumley, Woodhead Publishing, 2010.
- [7] Z. Xiong, I. Timokhina, E. Pereloma, Clustering, nano-scale precipitation and strengthening of steels, *Prog. Mater. Sci.* 118 (2021) 100764. <https://doi.org/10.1016/j.pmatsci.2020.100764>.
- [8] R. Kampmann, R. Wagner, in: *Mater. Sci. Technol. Compr. Treat.*, VCH, Weinheim, Germany, 1991: p. 213.
- [9] C. Dwyer, M. Weyland, L.Y. Chang, B.C. Muddle, Combined electron beam imaging and ab initio modeling of T(1) precipitates in Al-Li-Cu alloys, *Appl. Phys. Lett.* 98 (2011) 201909. <https://doi.org/10.1063/1.3590171>.
- [10] E.F. Rauch, M. Veron, Methods for orientation and phase identification of nano-sized embedded secondary phase particles by 4D scanning precession electron diffraction, *Acta Crystallogr. Sect. B-Struct. Sci. Cryst. Eng. Mater.* 75 (2019) 505–511. <https://doi.org/10.1107/S2052520619007583>.
- [11] J.K. Sunde, C.D. Marioara, A.T.J. van Helvoort, R. Holmestad, The evolution of precipitate crystal structures in an Al-Mg-Si(-Cu) alloy studied by a combined HAADF-STEM and SPED approach, *Mater. Charact.* 142 (2018) 458–469. <https://doi.org/10.1016/j.matchar.2018.05.031>.
- [12] T. Dorin, P. Donnadieu, J.-M. Chaix, W. Lefebvre, F. De Geuser, A. Deschamps, Size distribution and volume fraction of T-1 phase precipitates from TEM images: Direct measurements and related correction, *Micron.* 78 (2015) 19–27. <https://doi.org/10.1016/j.micron.2015.06.002>.
- [13] X. Xiong, M. Weyland, Microstructural Characterization of an Al-Li-Mg-Cu Alloy by Correlative Electron Tomography and Atom Probe Tomography, *Microsc. Microanal.* 20 (2014) 1022–1028. <https://doi.org/10.1017/S1431927614000798>.
- [14] C. Liu, S.K. Malladi, Q. Xu, J. Chen, F.D. Tichelaar, X. Zhuge, H.W. Zandbergen, In-situ STEM imaging of growth and phase change of individual CuAlX precipitates in Al alloy, *Sci. Rep.* 7 (2017) 2184. <https://doi.org/10.1038/s41598-017-02081-9>.
- [15] B. Gault, M.P. Moody, J.M. Cairney, S.P. Ringer, *Atom Probe Microscopy*, Springer, 2012.
- [16] B. Gault, A. Chiramonti, O. Cojocaru-Mirédin, P. Stender, R. Dubosq, C. Freysoldt, S.K. Makineni, T. Li, M. Moody, J.M. Cairney, Atom probe tomography, *Nat. Rev. Methods Primer.* 1

- (2021) 1–30. <https://doi.org/10.1038/s43586-021-00047-w>.
- [17] H. Zhao, B. Gault, D. Ponge, D. Raabe, F. De Geuser, Parameter free quantitative analysis of atom probe data by correlation functions: Application to the precipitation in Al-Zn-Mg-Cu, *Scr. Mater.* 154 (2018) 106–110. <https://doi.org/10.1016/j.scriptamat.2018.05.024>.
- [18] C.B. Fuller, J.L. Murray, D.N. Seidman, Temporal evolution of the nanostructure of Al(Sc,Zr) alloys: Part I - Chemical compositions of Al₃(Sc_{1-x}Zr_x) precipitates, *Acta Mater.* 53 (2005) 5401–5413.
- [19] V. Araullo-Peters, B. Gault, F. de Geuser, A. Deschamps, J.M. Cairney, Microstructural evolution during ageing of Al–Cu–Li–x alloys, *Acta Mater.* 66 (2014) 199–208. <https://doi.org/10.1016/j.actamat.2013.12.001>.
- [20] F. De Geuser, W. Lefebvre, Determination of Matrix Composition Based on Solute-Solute Nearest-Neighbor Distances in Atom Probe Tomography, *Microsc. Res. Tech.* 74 (2011) 257–263. <https://doi.org/10.1002/jemt.20899>.
- [21] F. De Geuser, B. Gault, Metrology of small particles and solute clusters by atom probe tomography, *Acta Mater.* 188 (2020) 406–415. <https://doi.org/10.1016/j.actamat.2020.02.023>.
- [22] C.E. Macchi, A. Somoza, A. Dupasquier, I.J. Polmear, Secondary precipitation in Al-Zn-Mg-(Ag) alloys, *Acta Mater.* 51 (2003) 5151–5158. [https://doi.org/10.1016/S1359-6454\(03\)00364-1](https://doi.org/10.1016/S1359-6454(03)00364-1).
- [23] J. Banhart, M.D.H. Lay, C.S.T. Chang, A.J. Hill, Kinetics of natural aging in Al-Mg-Si alloys studied by positron annihilation lifetime spectroscopy, *Phys. Rev. B.* 83 (2011) 014101. <https://doi.org/10.1103/PhysRevB.83.014101>.
- [24] B. Klobes, T.E.M. Staab, E. Dudzik, Early stages of decomposition in Al alloys investigated by X-ray absorption, *Phys. Status Solidi-Rapid Res. Lett.* 2 (2008) 182–184. <https://doi.org/10.1002/pssr.200802067>.
- [25] C. Hutchinson, P. Loo, T. Bastow, A. Hill, J. Teixeira, Quantifying the strain-induced dissolution of precipitates in Al alloy microstructures using nuclear magnetic resonance, *Acta Mater.* 57 (2009) 5645–5653. <https://doi.org/10.1016/j.actamat.2009.07.060>.
- [26] A. Deschamps, T.J. Bastow, F. De Geuser, A.J. Hill, C.R. Hutchinson, In-Situ Evaluation of the Microstructure Evolution during Rapid Hardening of an Al-2.5Cu-1.5Mg (wt. %) Alloy, *Acta Mater.* 59 (2011) 2918–2927.
- [27] G. Meyruey, V. Massardier, W. Lefebvre, M. Perez, Over-ageing of an Al-Mg-Si alloy with silicon excess, *Mater. Sci. Eng. -Struct. Mater. Prop. Microstruct. Process.* 730 (2018) 92–105. <https://doi.org/10.1016/j.msea.2018.05.094>.
- [28] F. De Geuser, A. Deschamps, Precipitate characterisation in metallic systems by small-angle X-ray or neutron scattering, *Comptes Rendus Phys.* 13 (2012) 246–256. <https://doi.org/10.1016/j.crhy.2011.12.008>.
- [29] A. Deschamps, F. De Geuser, Quantitative Characterization of Precipitate Microstructures in Metallic Alloys Using Small-Angle Scattering, *Metall. Mater. Trans. -Phys. Metall. Mater. Sci.* 44A (2013) 77–86. <https://doi.org/10.1007/s11661-012-1435-7>.
- [30] G. Spartacus, J. Malaplate, F. De Geuser, D. Sornin, A. Gangloff, R. Guillou, A. Deschamps, Nano-oxide precipitation kinetics during the consolidation process of a ferritic oxide dispersion strengthened steel., *Scr. Mater.* 188 (2020) 10–15. <https://doi.org/10.1016/j.scriptamat.2020.07.003>.
- [31] A. Deschamps, G. Fribourg, Y. Brechet, J.L. Chemin, C.R. Hutchinson, In situ evaluation of dynamic precipitation during plastic straining of an Al-Zn-Mg-Cu alloy, *Acta Mater.* 60 (2012) 1905–1916. <https://doi.org/10.1016/j.actamat.2012.01.002>.
- [32] J.F. dos Santos, P. Staron, T. Fischer, J.D. Robson, A. Kostka, P. Colegrove, H. Wang, J. Hilgert, L. Bergmann, L.L. Huetsch, N. Huber, A. Schreyer, Understanding precipitate evolution during friction stir welding of Al-Zn-Mg-Cu alloy through in-situ measurement coupled with simulation, *Acta Mater.* 148 (2018) 163–172. <https://doi.org/10.1016/j.actamat.2018.01.020>.
- [33] O. Tissot, C. Pareige, M.-H. Mathon, M. Roussel, E. Meslin, B. Decamps, J. Henry, Comparison between SANS and APT measurements in a thermally aged Fe-19 at.%Cr alloy, *Mater.*

- Charact. 151 (2019) 332–341. <https://doi.org/10.1016/j.matchar.2019.03.027>.
- [34] M. Ohnuma, J. Suzuki, S. Ohtsuka, S.-W. Kim, T. Kaito, M. Inoue, H. Kitazawa, A new method for the quantitative analysis of the scale and composition of nanosized oxide in 9Cr-ODS steel, *Acta Mater.* 57 (2009) 5571–5581. <https://doi.org/10.1016/j.actamat.2009.07.054>.
- [35] J. Coakley, B.-S. Seong, D. Dye, M. Ohnuma, Isothermal omega kinetics in beta-titanium alloys, *Philos. Mag. Lett.* 97 (2017) 83–91. <https://doi.org/10.1080/09500839.2017.1282633>.
- [36] R. Ivanov, A. Deschamps, F. De Geuser, Clustering kinetics during natural ageing of Al-Cu based alloys with (Mg, Li) additions, *Acta Mater.* 157 (2018) 186–195. <https://doi.org/10.1016/j.actamat.2018.07.035>.
- [37] T. Marlaud, A. Deschamps, F. Bley, W. Lefebvre, B. Baroux, Influence of alloy composition and heat treatment on precipitate composition in Al-Zn-Mg-Cu alloys, *Acta Mater.* 58 (2010) 248–260.
- [38] M. Dumont, L. Commin, I. Morfin, F. De Geuser, F. Legendre, P. Maugis, Chemical composition of nano-phases studied by anomalous small-angle X-ray: Application to oxide nanoparticles in ODS steels (vol 87, pg 138, 2013), *Mater. Charact.* 102 (2015) 221–221. <https://doi.org/10.1016/j.matchar.2015.02.007>.
- [39] M.J. Styles, R.K.W. Marceau, T.J. Bastow, H.E.A. Brand, M.A. Gibson, C.R. Hutchinson, The competition between metastable and equilibrium S (Al₂CuMg) phase during the decomposition of AlCuMg alloys, *Acta Mater.* 98 (2015) 64–80. <https://doi.org/10.1016/j.actamat.2015.07.011>.
- [40] M.S. Blackmur, J.D. Robson, M. Preuss, O. Zanellato, R.J. Cernik, S.-Q. Shi, F. Ribeiro, J. Andrieux, Zirconium hydride precipitation kinetics in Zircaloy-4 observed with synchrotron X-ray diffraction, *J. Nucl. Mater.* 464 (2015) 160–169. <https://doi.org/10.1016/j.jnucmat.2015.04.025>.
- [41] D.M. Collins, D.J. Crudden, E. Alabort, T. Connolley, R.C. Reed, Time-resolved synchrotron diffractometry of phase transformations in high strength nickel-based superalloys, *Acta Mater.* 94 (2015) 244–256. <https://doi.org/10.1016/j.actamat.2015.04.046>.
- [42] L.D. Connor, P.M. Mignanelli, K.A. Christofidou, N.G. Jones, A.R. Baker, C.C. Tang, S. Guerin, H.J. Stone, In situ study of sigma phase formation in Cr-Co-Ni ternary alloys at 800 degrees C using the long duration experiment facility at Diamond Light Source, *J. Synchrotron Radiat.* 25 (2018) 1371–1378. <https://doi.org/10.1107/S1600577518009475>.
- [43] F. Zhang, L.E. Levine, A.J. Allen, C.E. Campbell, A.A. Creuziger, N. Kazantseva, J. Ilavsky, In situ structural characterization of ageing kinetics in aluminum alloy 2024 across angstrom-to-micrometer length scales, *Acta Mater.* 111 (2016) 385–398. <https://doi.org/10.1016/j.actamat.2016.03.058>.
- [44] R.N. Andrews, J. Serio, G. Muralidharan, J. Ilavsky, An in situ USAXS-SAXS-WAXS study of precipitate size distribution evolution in a model Ni-based alloy, *J. Appl. Crystallogr.* 50 (2017) 734–740. <https://doi.org/10.1107/S1600576717006446>.
- [45] S. Haas, J. Andersson, M. Fisk, J.-S. Park, U. Lienert, Correlation of precipitate evolution with Vickers hardness in Haynes® 282® superalloy: In-situ high-energy SAXS/WAXS investigation, *Mater. Sci. Eng. A.* 711 (2018) 250–258. <https://doi.org/10.1016/j.msea.2017.11.035>.
- [46] T. Dorin, A. Deschamps, F. De Geuser, W. Lefebvre, C. Sigli, Quantitative description of the T1 formation kinetics in an Al–Cu–Li alloy using differential scanning calorimetry, small-angle X-ray scattering and transmission electron microscopy, *Philos. Mag.* 94 (2014) 1012–1030. <https://doi.org/10.1080/14786435.2013.878047>.
- [47] S. Esmaeili, D.J. Lloyd, Modeling of precipitation hardening in pre-aged AlMgSi(Cu) alloys, *Acta Mater.* 53 (2005) 5257–5271. <https://doi.org/10.1016/j.actamat.2005.08.006>.
- [48] B. Yang, B. Milkereit, Y. Zhang, P.A. Rometsch, O. Kessler, C. Schick, Continuous cooling precipitation diagram of aluminium alloy AA7150 based on a new fast scanning calorimetry and interrupted quenching method, *Mater. Charact.* 120 (2016) 30–37. <https://doi.org/10.1016/j.matchar.2016.08.016>.
- [49] H. Froeck, M. Reich, B. Milkereit, O. Kessler, Scanning Rate Extension of Conventional DSCs through Indirect Measurements, *Materials.* 12 (2019) 1085. <https://doi.org/10.3390/ma12071085>.

- [50] B. Milkereit, M.J. Starink, P.A. Rometsch, C. Schick, O. Kessler, Review of the Quench Sensitivity of Aluminium Alloys: Analysis of the Kinetics and Nature of Quench-Induced Precipitation, *Materials*. 12 (2019) 4083. <https://doi.org/10.3390/ma12244083>.
- [51] I.-E. Benrabah, G. Altinkurt, M. Fevre, M. Dehmas, B. Denand, F. Fossard, J.-S. Merot, G. Geandier, D. Locq, M. Perrut, Monitoring the kinetics of the gamma ' phase in the N18 superalloy using in situ electrical resistivity measurements, *J. Alloys Compd.* 825 (2020) 154108. <https://doi.org/10.1016/j.jallcom.2020.154108>.
- [52] F. Jiang, H.S. Zurob, G.R. Purdy, H. Zhang, Characterizing precipitate evolution of an Al–Zn–Mg–Cu-based commercial alloy during artificial aging and non-isothermal heat treatments by in situ electrical resistivity monitoring, *Mater. Charact.* 117 (2016) 47–56. <https://doi.org/10.1016/j.matchar.2016.04.014>.
- [53] H. Seyedrezai, D. Grebennikov, P. Mascher, H.S. Zurob, Study of the early stages of clustering in Al-Mg-Si alloys using the electrical resistivity measurements, *Mater. Sci. Eng. -Struct. Mater. Prop. Microstruct. Process.* 525 (2009) 186–191. <https://doi.org/10.1016/j.msea.2009.06.054>.
- [54] R. Enzinger, E. Hengge, W. Sprengel, R. Wuerschum, High-precision isothermal dilatometry as tool for quantitative analysis of precipitation kinetics: case study of dilute Al alloy, *J. Mater. Sci.* 54 (2019) 5083–5091. <https://doi.org/10.1007/s10853-018-03210-z>.
- [55] C.S. Kaira, V. De Andrade, S.S. Singh, C. Kantzos, A. Kirubanandham, F. De Carlo, N. Chawla, Probing Novel Microstructural Evolution Mechanisms in Aluminum Alloys Using 4D Nanoscale Characterization, *Adv. Mater.* 29 (2017) 1703482. <https://doi.org/10.1002/adma.201703482>.
- [56] K. Russell, Nucleation in Solids - the Induction and Steady-State Effects, *Adv. Colloid Interface Sci.* 13 (1980) 205–318. [https://doi.org/10.1016/0001-8686\(80\)80003-0](https://doi.org/10.1016/0001-8686(80)80003-0).
- [57] H.I. Aaronson, J.K. Lee, The kinetic equations of solid-solid nucleation theory and comparisons with experimental observations, in: *Lect. Theory Phase Transform.* 2nd Ed, Aaronson HI, The Minerals, Metals and Materials Society (TMS)., Warrendale, 1999.
- [58] E. Clouet, M. Nastar, C. Sigli, Nucleation of Al₃Zr and Al₃Sc in aluminum alloys: From kinetic Monte Carlo simulations to classical theory, *Phys. Rev. B Condens. Matter Mater. Phys.* 69 (2004) 064109/1-064109/14.
- [59] K.F. Kelton, A.F. Greer, *Nucleation in Condensed Matter – Applications in Materials and Biology*, Pergamon, Amsterdam, 2010.
- [60] C. Zener, *J. Appl. Phys.* 20 (1949) 950–953.
- [61] R. Kampmann, R. Wagner, Kinetics of precipitation in metastable binary alloys – theory and application to Cu-1.9 at.% Ti and Ni-14 at. % Al, in: *Decompos. Alloys Early Stages*, Pergamon Press, Oxford, 1984.
- [62] M. Perez, M. Dumont, D. Acevedo-Reyes, Implementation of classical nucleation and growth theories for precipitation, *Acta Mater.* 56 (2008) 2119–2132.
- [63] R. Rettig, R.F. Singer, Numerical modelling of precipitation of topologically close-packed phases in nickel-base superalloys, *Acta Mater.* 59 (2011) 317–327. <https://doi.org/10.1016/j.actamat.2010.09.035>.
- [64] E. Povoden-Karadeniz, E. Kozeschnik, Simulation of Precipitation Kinetics and Precipitation Strengthening of B2-precipitates in Martensitic PH 13-8 Mo Steel, *Isij Int.* 52 (2012) 610–615. <https://doi.org/10.2355/isijinternational.52.610>.
- [65] Z. Hou, P. Hedström, Q. Chen, Y. Xu, D. Wu, J. Odqvist, Quantitative modeling and experimental verification of carbide precipitation in a martensitic Fe–0.16wt% C–4.0wt% Cr alloy, *Calphad.* 53 (2016) 39–48. <https://doi.org/10.1016/j.calphad.2016.03.001>.
- [66] X. Xia, W. Sun, A.A. Luo, D.S. Stone, Precipitation evolution and hardening in MgSmZnZr alloys, *Acta Mater.* 111 (2016) 335–347. <https://doi.org/10.1016/j.actamat.2016.03.068>.
- [67] M.R. Ahmadi, M. Rath, E. Povoden-Karadeniz, S. Primig, T. Wojcik, A. Danninger, M. Stockinger, E. Kozeschnik, Modeling of precipitation strengthening in Inconel 718 including non-spherical gamma ' ' precipitates, *Model. Simul. Mater. Sci. Eng.* 25 (2017) 055005.

<https://doi.org/10.1088/1361-651X/aa6f54>.

- [68] R. Shi, A.A. Luo, Applications of CALPHAD modeling and databases in advanced lightweight metallic materials, *Calphad-Comput. Coupling Phase Diagr. Thermochem.* 62 (2018) 1–17. <https://doi.org/10.1016/j.calphad.2018.04.009>.
- [69] A. Deschamps, Y. Brechet, Influence of predeformation and ageing of an Al-Zn-Mg alloy - II. Modeling of precipitation kinetics and yield stress, *Acta Mater.* 47 (1999) 293–305.
- [70] I.M. Lifshitz, V.V. Slyozov, The kinetics of precipitation from supersaturated solid solutions, *J. Phys. Chem. Solids.* 19 (1961) 35–50.
- [71] C. Wagner, Theory of precipitate change by redissolution, *Z. Für Elektrochem.* 65 (1961) 581–591.
- [72] M. HILLERT, The role of interfacial energy during solid-state phase transformations, *Jernkontorets Ann.* 141 (1957) 757–789.
- [73] M. Hillert, L. Hoglund, J. Agren, Diffusion-controlled lengthening of Widmanstätten plates, *Acta Mater.* 51 (2003) 2089–2095. [https://doi.org/10.1016/S1359-6454\(03\)00008-9](https://doi.org/10.1016/S1359-6454(03)00008-9).
- [74] L. Leach, J. Agren, L. Hoglund, A. Borgenstam, Diffusion-Controlled Lengthening Rates of Bainitic Ferrite a Part of the Steel Genome, *Metall. Mater. Trans. -Phys. Metall. Mater. Sci.* 50A (2019) 2613–2618. <https://doi.org/10.1007/s11661-019-05208-x>.
- [75] E. Clouet, A. Barbu, L. Lae, G. Martin, Precipitation kinetics of Al₃Zr and Al₃Sc in aluminum alloys modeled with cluster dynamics, *Acta Mater.* 53 (2005) 2313–2325.
- [76] A. Barbu, E. Clouet, Cluster dynamics modeling of materials: Advantages and limitations, in: R. Kozubski, G.E. Murch, P. Zieba (Eds.), *Multiscale Kinet. Model. Mater.*, Trans Tech Publications Ltd, Durnten-Zurich, 2007: pp. 51–+. <https://doi.org/10.4028/www.scientific.net/SSP.129.51>.
- [77] T. Stegmüller, F. Haider, Multi-scale Cluster Dynamics modelling of Guinier-Preston zone formation in binary Al-Cu alloys, *Acta Mater.* 177 (2019) 240–249. <https://doi.org/10.1016/j.actamat.2019.07.032>.
- [78] J.Z. Zhu, T. Wang, A.J. Ardell, S.H. Zhou, Z.K. Liu, L.Q. Chen, Three-dimensional phase-field simulations of coarsening kinetics of gamma ' particles in binary Ni-Al alloys, *Acta Mater.* 52 (2004) 2837–2845. <https://doi.org/10.1016/j.actamat.2004.02.032>.
- [79] Y. Song, B. Radhakrishnan, S. Gorti, R. Acharya, Precipitate growth kinetics under inhomogeneous concentration fields using a phase-field model, *Phys. Rev. Mater.* 5 (2021) 053401. <https://doi.org/10.1103/PhysRevMaterials.5.053401>.
- [80] C.O. Yenusah, Y. Ji, Y. Liu, T.W. Stone, M.F. Horstemeyer, L.-Q. Chen, L. Chen, Three-dimensional Phase-field simulation of gamma ' ' precipitation kinetics in Inconel 625 during heat treatment, *Comput. Mater. Sci.* 187 (2021) 110123. <https://doi.org/10.1016/j.commatsci.2020.110123>.
- [81] L.Q. Chen, Phase-field models for microstructure evolution, *Annu. Rev. Mater. Res.* 32 (2002) 113–140. <https://doi.org/10.1146/annurev.matsci.32.112001.132041>.
- [82] N. Moelans, B. Blanpain, P. Wollants, An introduction to phase-field modeling of microstructure evolution, *Calphad-Comput. Coupling Phase Diagr. Thermochem.* 32 (2008) 268–294. <https://doi.org/10.1016/j.calphad.2007.11.003>.
- [83] E. Clouet, M. Nastar, A. Barbu, C. Sigli, G. Martin, Precipitation in Al-Zr-Sc alloys: a comparison between kinetic Monte Carlo, cluster dynamics and classical nucleation theory, *Minerals, Metals & Materials Soc, Warrendale*, 2005.
- [84] E. Clouet, L. Lae, T. Epicier, W. Lefebvre, M. Nastar, A. Deschamps, Complex precipitation pathways in multi-component alloys, *Nat. Mater.* 5 (2006) 482–488.
- [85] E.A. Marquis, J.M. Hyde, Applications of atom-probe tomography to the characterisation of solute behaviours, *Mater. Sci. Eng. R-Rep.* 69 (2010) 37–62. <https://doi.org/10.1016/j.mser.2010.05.001>.
- [86] L. Couturier, F. De Geuser, A. Deschamps, Direct comparison of Fe-Cr unmixing characterization by atom probe tomography and small angle scattering, *Mater. Charact.* 121 (2016) 61–67. <https://doi.org/10.1016/j.matchar.2016.09.028>.

- [87] A. Lervik, E. Thronsen, J. Friis, C.D. Marioara, S. Wenner, A. Bendo, K. Matsuda, R. Holmestad, S.J. Andersen, Atomic structure of solute clusters in Al-Zn-Mg alloys, *Acta Mater.* 205 (2021) 116574. <https://doi.org/10.1016/j.actamat.2020.116574>.
- [88] B. Wattiez, A.F. Gourgues, A. Deschamps, A. Roemer, Z. Zermout, Experimental investigation of microstructure and ageing behaviour of bulk Zn-(1–18)wt% Al-(0–0.06)wt% Mg alloys, *Mater. Sci. Eng. A.* 527 (2010) 7901–7911. <https://doi.org/10.1016/j.msea.2010.08.068>.
- [89] F. De Geuser, M.J. Styles, C.R. Hutchinson, A. Deschamps, High-throughput in-situ characterization and modeling of precipitation kinetics in compositionally graded alloys, *Acta Mater.* 101 (2015) 1–9. <https://doi.org/10.1016/j.actamat.2015.08.061>.
- [90] W.W. Sun, R.K.W. Marceau, M.J. Styles, D. Barbier, C.R. Hutchinson, G phase precipitation and strengthening in ultra-high strength ferritic steels: Towards lean ‘maraging’ metallurgy, *Acta Mater.* 130 (2017) 28–46. <https://doi.org/10.1016/j.actamat.2017.03.032>.
- [91] F. Soisson, G. Martin, Monte Carlo simulations of the decomposition of metastable solid solutions: Transient and steady-state nucleation kinetics, *Phys. Rev. B.* 62 (2000) 203–214. <https://doi.org/10.1103/PhysRevB.62.203>.
- [92] E. Clouet, M. Nastar, Classical nucleation theory in ordering alloys precipitating with L12 structure, *Phys. Rev. B.* 75 (2007) 132102. <https://doi.org/10.1103/PhysRevB.75.132102>.
- [93] E.A. Marquis, D.N. Seidman, Nanoscale structural evolution of Al₃Sc precipitates in Al(Sc) alloys, *Acta Mater.* 49 (2001) 1909–1919.
- [94] T. Jourdan, F. Soisson, E. Clouet, A. Barbu, Influence of cluster mobility on Cu precipitation in α -Fe: A cluster dynamics modeling, *Acta Mater.* 58 (2010) 3400–3405. <https://doi.org/10.1016/j.actamat.2010.02.014>.
- [95] M. Perrier, A. Deschamps, O. Bouaziz, Y. Brechet, F. Danoix, F. De Geuser, P. Donnadieu, K. Houmada, P. Maugis, Characterization and Modeling of Precipitation Kinetics in a Fe-Si-Ti Alloy, *Metall. Mater. Trans. -Phys. Metall. Mater. Sci.* 43A (2012) 4999–5008. <https://doi.org/10.1007/s11661-012-1337-8>.
- [96] J. Banhart, C.S.T. Chang, Z. Liang, N. Wanderka, M.D.H. Lay, A.J. Hill, Natural Aging in Al-Mg-Si Alloys - A Process of Unexpected Complexity, *Adv. Eng. Mater.* 12 (2010) 559–571. <https://doi.org/10.1002/adem.201000041>.
- [97] S. Pogatscher, H. Antrekowitsch, M. Werinos, F. Moszner, S.S.A. Gerstl, M.F. Francis, W.A. Curtin, J.F. Loeffler, P.J. Uggowitzer, Diffusion on Demand to Control Precipitation Aging: Application to Al-Mg-Si Alloys, *Phys. Rev. Lett.* 112 (2014) 225701. <https://doi.org/10.1103/PhysRevLett.112.225701>.
- [98] M.F. Francis, W.A. Curtin, Microalloying for the controllable delay of precipitate formation in metal alloys, *Acta Mater.* 106 (2016) 117–128. <https://doi.org/10.1016/j.actamat.2016.01.014>.
- [99] P. Dumitraschkewitz, P.J. Uggowitzer, S.S.A. Gerstl, J.F. Loeffler, S. Pogatscher, Size-dependent diffusion controls natural aging in aluminium alloys, *Nat. Commun.* 10 (2019) 4746. <https://doi.org/10.1038/s41467-019-12762-w>.
- [100] F. Lotter, D. Petschke, F. De Geuser, M. Elsayed, G. SEXTL, T.E.M. Staab, In situ natural ageing of Al-Cu-(Mg) alloys: The effect of In and Sn on the very early stages of decomposition, *Scr. Mater.* 168 (2019) 104–107. <https://doi.org/10.1016/j.scriptamat.2019.04.031>.
- [101] Y.X. Wu, W.W. Sun, M.J. Styles, A. Arlazarov, C.R. Hutchinson, Cementite coarsening during the tempering of Fe-C-Mn martensite, *Acta Mater.* 159 (2018) 209–224. <https://doi.org/10.1016/j.actamat.2018.08.023>.
- [102] Y.X. Wu, W.W. Sun, X. Gao, M.J. Styles, A. Arlazarov, C.R. Hutchinson, The effect of alloying elements on cementite coarsening during martensite tempering, *Acta Mater.* 183 (2020) 418–437. <https://doi.org/10.1016/j.actamat.2019.11.040>.
- [103] S. Pogatscher, H. Antrekowitsch, H. Leitner, D. Pöschmann, Z.L. Zhang, P.J. Uggowitzer, Influence of interrupted quenching on artificial aging of Al-Mg-Si alloys, *Acta Mater.* 60 (2012) 4496–4505. <https://doi.org/10.1016/j.actamat.2012.04.026>.
- [104] P. Schloth, A. Deschamps, Ch.-A. Gandin, J.-M. Drezet, Modeling of GP(I) zone formation during quench in an industrial AA7449 75 mm thick plate, *Mater. Des.* 112 (2016) 46–57.

<https://doi.org/10.1016/j.matdes.2016.09.052>.

- [105] M. Madanat, M. Liu, J. Banhart, Reversion of natural ageing in Al-Mg-Si alloys, *Acta Mater.* 159 (2018) 163–172. <https://doi.org/10.1016/j.actamat.2018.07.066>.
- [106] Z. Yang, X. Jiang, X. Zhang, M. Liu, Z. Liang, D. Leyvraz, J. Banhart, Natural ageing clustering under different quenching conditions in an Al-Mg-Si alloy, *Scr. Mater.* 190 (2021) 179–182. <https://doi.org/10.1016/j.scriptamat.2020.08.046>.
- [107] C.R. Hutchinson, B.M. Gable, N. Ciccossillo, P.T. Loo, T.J. Bastow, A.J. Hill, An experimental determination of solute-vacancy binding energies in high purity dilute Al-X alloys, in: *Alum. Alloys Their Phys. Mech. Prop.*, J. Hirsch, B. Skrotzki and G. Gottstein, Eds, Wiley-VCH, 2008: pp. 788–794.
- [108] F. Soisson, C.-C. Fu, Cu-precipitation kinetics in alpha-Fe from atomistic simulations: Vacancy-trapping effects and Cu-cluster mobility, *Phys. Rev. B.* 76 (2007) 214102. <https://doi.org/10.1103/PhysRevB.76.214102>.
- [109] T. Jourdan, J.-L. Bocquet, F. Soisson, Modeling homogeneous precipitation with an event-based Monte Carlo method: Application to the case of Fe-Cu, *Acta Mater.* 58 (2010) 3295–3302. <https://doi.org/10.1016/j.actamat.2010.02.003>.
- [110] H.S. Zurob, H. Seyedrezai, A model for the growth of solute clusters based on vacancy trapping, *Scr. Mater.* 61 (2009) 141–144. <https://doi.org/10.1016/j.scriptamat.2009.03.025>.
- [111] M.D.H. Lay, H.S. Zurob, C.R. Hutchinson, T.J. Bastow, A.J. Hill, Vacancy Behavior and Solute Cluster Growth During Natural Aging of an Al-Mg-Si Alloy, *Metall. Mater. Trans. -Phys. Metall. Mater. Sci.* 43A (2012) 4507–4513. <https://doi.org/10.1007/s11661-012-1257-7>.
- [112] L.A. Girifalco, H. Herman, *Acta Metall.* 13 (1965) 583.
- [113] Z. Mao, C.K. Sudbrack, K.E. Yoon, G. Martin, D.N. Seidman, Themechanism of morphogenesis in a phase-separating concentrated multicomponent alloy, *Nat. Mater.* 6 (2007) 210–216. <https://doi.org/10.1038/nmat1845>.
- [114] Z. Mao, C. Booth-Morrison, C.K. Sudbrack, G. Martin, D.N. Seidman, Kinetic pathways for phase separation: An atomic-scale study in Ni-Al-Cr alloys, *Acta Mater.* 60 (2012) 1871–1888. <https://doi.org/10.1016/j.actamat.2011.10.046>.
- [115] J. Lepinoux, C. Sigli, Precipitate growth in concentrated binary alloys: a comparison between kinetic Monte Carlo simulations, cluster dynamics and the classical theory, *Philos. Mag.* 93 (2013) 3194–3215. <https://doi.org/10.1080/14786435.2013.805275>.
- [116] J. Lepinoux, C. Sigli, On the effect of concentrated solid solutions on properties of clusters in a model binary alloy, *Philos. Mag.* 96 (2016) 955–971. <https://doi.org/10.1080/14786435.2016.1149246>.
- [117] J. Lepinoux, C. Sigli, Extracting free energy of clusters in concentrated binary alloys from atomistic Monte Carlo simulations, *Model. Simul. Mater. Sci. Eng.* 27 (2019) 085001. <https://doi.org/10.1088/1361-651X/ab3ef9>.
- [118] J.D. Robson, Modelling the overlap of nucleation, growth and coarsening during precipitation, *Acta Mater.* 52 (2004) 4669–4676.
- [119] A. Seret, C. Moussa, M. Bernacki, N. Bozzolo, A mean field model of agglomeration as an extension to existing precipitation models, *Acta Mater.* 192 (2020) 40–51. <https://doi.org/10.1016/j.actamat.2020.04.029>.
- [120] A.J. Ardell, The effect of volume fraction on particle coarsening: theoretical considerations, *Acta Metall.* 20 (1972) 61–71. [https://doi.org/10.1016/0001-6160\(72\)90114-9](https://doi.org/10.1016/0001-6160(72)90114-9).
- [121] C. Davies, P. Nash, R. Stevens, Effect of Volume Fraction of Precipitate on Ostwald Ripening, *Acta Metall.* 28 (1980) 179–189. [https://doi.org/10.1016/0001-6160\(80\)90067-X](https://doi.org/10.1016/0001-6160(80)90067-X).
- [122] H.A. Calderon, P.W. Voorhees, J.L. Murray, G. Kostorz, Ostwald ripening in concentrated alloys, *Acta Metall. Mater.* 42 (1994) 991–1000. [https://doi.org/10.1016/0956-7151\(94\)90293-3](https://doi.org/10.1016/0956-7151(94)90293-3).
- [123] A.J. Ardell, Quantitative predictions of the trans-interface diffusion-controlled theory of particle coarsening, *Acta Mater.* 58 (2010) 4325–4331. <https://doi.org/10.1016/j.actamat.2010.04.018>.
- [124] T. Philippe, P.W. Voorhees, Ostwald ripening in multicomponent alloys, *Acta Mater.* 61

- (2013) 4237–4244. <https://doi.org/10.1016/j.actamat.2013.03.049>.
- [125] P. Streitenberger, Analytical description of phase coarsening at high volume fractions, *Acta Mater.* 61 (2013) 5026–5035. <https://doi.org/10.1016/j.actamat.2013.04.042>.
- [126] K. Kim, P.W. Voorhees, Ostwald ripening of spheroidal particles in multicomponent alloys, *Acta Mater.* 152 (2018) 327–337. <https://doi.org/10.1016/j.actamat.2018.04.041>.
- [127] T. Philippe, D. Blavette, Nucleation pathway in coherent precipitation, *Philos. Mag.* 91 (2011) 4606–4622. <https://doi.org/10.1080/14786435.2011.616548>.
- [128] M. Bonvalet, T. Philippe, X. Sauvage, D. Blavette, The influence of size on the composition of nano-precipitates in coherent precipitation, *Philos. Mag.* 94 (2014) 2956–2966. <https://doi.org/10.1080/14786435.2014.941029>.
- [129] P. Maugis, M. Gouné, Kinetics of vanadium carbonitride precipitation in steel: A computer model, *Acta Mater.* 53 (2005) 3359–3367. <https://doi.org/10.1016/j.actamat.2005.03.036>.
- [130] T. Marlaud, A. Deschamps, F. Bley, W. Lefebvre, B. Baroux, Evolution of precipitate microstructures during the retrogression and re-ageing heat treatment of an Al–Zn–Mg–Cu alloy, *Acta Mater.* 58 (2010) 4814–4826. <https://doi.org/10.1016/j.actamat.2010.05.017>.
- [131] C. Booth-Morrison, D.C. Dunand, D.N. Seidman, Coarsening resistance at 400°C of precipitation-strengthened Al–Zr–Sc–Er alloys, *Acta Mater.* 59 (2011) 7029–7042. <https://doi.org/10.1016/j.actamat.2011.07.057>.
- [132] V. Radmilovic, C. Ophus, E.A. Marquis, M.D. Rossell, A. Tolley, A. Gautam, M. Asta, U. Dahmen, Highly monodisperse core-shell particles created by solid-state reactions, *Nat. Mater.* 10 (2011) 710–715. <https://doi.org/10.1038/NMAT3077>.
- [133] C. Booth-Morrison, Z. Mao, M. Diaz, D.C. Dunand, C. Wolverton, D.N. Seidman, Role of silicon in accelerating the nucleation of Al₃(Sc,Zr) precipitates in dilute Al–Sc–Zr alloys, *Acta Mater.* 60 (2012) 4740–4752. <https://doi.org/10.1016/j.actamat.2012.05.036>.
- [134] A. De Luca, D.C. Dunand, D.N. Seidman, Microstructure and mechanical properties of a precipitation-strengthened Al–Zr–Sc–Er–Si alloy with a very small Sc content, *Acta Mater.* 144 (2018) 80–91. <https://doi.org/10.1016/j.actamat.2017.10.040>.
- [135] S. Shu, P.B. Wells, N. Almirall, G.R. Odette, D.D. Morgan, Thermodynamics and kinetics of core-shell versus appendage co-precipitation morphologies: An example in the Fe–Cu–Mn–Ni–Si system, *Acta Mater.* 157 (2018) 298–306. <https://doi.org/10.1016/j.actamat.2018.07.037>.
- [136] A. Deschamps, L. Lae, P. Guyot, In situ small-angle scattering study of the precipitation kinetics in an Al–Zr–Sc alloy, *Acta Mater.* 55 (2007) 2775–2783.
- [137] M.E. van Dalen, T. Gyger, D.C. Dunand, D.N. Seidman, Effects of Yb and Zr microalloying additions on the microstructure and mechanical properties of dilute Al–Sc alloys, *Acta Mater.* 59 (2011) 7615–7626. <https://doi.org/10.1016/j.actamat.2011.09.019>.
- [138] B. Forbord, W. Lefebvre, F. Danoix, H. Hallem, K. Marthinsen, Three dimensional atom probe investigation on the formation of Al₃(Sc,Zr)-dispersoids in aluminium alloys, *Scr. Mater.* 51 (2004) 333–337.
- [139] Z. Mao, C.K. Sudbrack, K.E. Yoon, G. Martin, D.N. Seidman, Themechanism of morphogenesis in a phase-separating concentrated multicomponent alloy, *Nat. Mater.* 6 (2007) 210–216. <https://doi.org/10.1038/nmat1845>.
- [140] C. Booth-Morrison, R.D. Noebe, D.N. Seidman, Effects of tantalum on the temporal evolution of a model Ni–Al–Cr superalloy during phase decomposition, *Acta Mater.* 57 (2009) 909–920. <https://doi.org/10.1016/j.actamat.2008.10.029>.
- [141] J. Svoboda, F.D. Fischer, P. Fratzl, E. Kozeschnik, Modelling of kinetics in multi-component multi-phase systems with spherical precipitates: I: Theory, *Mater. Sci. Eng. A.* 385 (2004) 166–174. <https://doi.org/10.1016/j.msea.2004.06.018>.
- [142] Q. Du, W.J. Poole, M.A. Wells, A mathematical model coupled to CALPHAD to predict precipitation kinetics for multicomponent aluminum alloys, *Acta Mater.* 60 (2012) 3830–3839. <https://doi.org/10.1016/j.actamat.2012.02.050>.
- [143] Q. Du, J. Friis, Modeling precipitate growth in multicomponent alloy systems by a variational principle, *Acta Mater.* 64 (2014) 411–418.

<https://doi.org/10.1016/j.actamat.2013.10.054>.

[144] M. Bonvalet, T. Philippe, X. Sauvage, D. Blavette, Modeling of precipitation kinetics in multicomponent systems: Application to model superalloys, *Acta Mater.* 100 (2015) 169–177.

<https://doi.org/10.1016/j.actamat.2015.08.041>.

[145] M.J. Anderson, A. Rowe, J. Wells, H.C. Basoalto, Application of a multi-component mean field model to the coarsening behaviour of a nickel-based superalloy, *Acta Mater.* 114 (2016) 80–96. <https://doi.org/10.1016/j.actamat.2016.05.024>.

[146] L. Rougier, A. Jacot, C.-A. Gandin, D. Ponsen, V. Jaquet, Numerical Simulation of Solidification, Homogenization, and Precipitation in an Industrial Ni-Based Superalloy, *Metall. Mater. Trans. -Phys. Metall. Mater. Sci.* 47A (2016) 5557–5568. <https://doi.org/10.1007/s11661-016-3694-1>.

[147] I.J. Moore, M.G. Burke, E.J. Palmiere, Modelling the nucleation, growth and coarsening kinetics of γ' ($\text{D0}(22)$) precipitates in the Ni-base Alloy 625, *Acta Mater.* 119 (2016) 157–166. <https://doi.org/10.1016/j.actamat.2016.08.027>.

[148] M.J. Anderson, C. Panwisawas, Y. Sovani, R.P. Turner, J.W. Brooks, H.C. Basoalto, Mean-field modelling of the intermetallic precipitate phases during heat treatment and additive manufacture of Inconel 718, *Acta Mater.* 156 (2018) 432–445.

<https://doi.org/10.1016/j.actamat.2018.07.002>.

[149] A. Azzam, T. Philippe, A. Hauet, F. Danoix, D. Locq, P. Caron, D. Blavette, Kinetics pathway of precipitation in model Co-Al-W superalloy, *Acta Mater.* 145 (2018) 377–387.

<https://doi.org/10.1016/j.actamat.2017.12.032>.

[150] M. Bonvalet-Rolland, T. Philippe, J. Agren, Kinetic theory of nucleation in multicomponent systems: An application of the thermodynamic extremum principle, *Acta Mater.* 171 (2019) 1–7.

<https://doi.org/10.1016/j.actamat.2019.03.031>.

[151] W.E. Frazier, T.G. Lach, T.S. Byun, Monte Carlo simulations of Cu/Ni-Si-Mn co-precipitation in duplex stainless steels, *Acta Mater.* 194 (2020) 1–12.

<https://doi.org/10.1016/j.actamat.2020.03.053>.

[152] S.B. Kadambi, F. Abdeljawad, S. Patala, Interphase boundary segregation and precipitate coarsening resistance in ternary alloys: An analytic phase-field model describing chemical effects, *Acta Mater.* 197 (2020) 283–299. <https://doi.org/10.1016/j.actamat.2020.06.052>.

[153] J.M. Rosalie, L. Bourgeois, Silver segregation to θ' (Al_2Cu)-Al interfaces in Al-Cu-Ag alloys, *Acta Mater.* 60 (2012) 6033–6041. <https://doi.org/10.1016/j.actamat.2012.07.039>.

[154] C. Yang, P. Zhang, D. Shao, R.H. Wang, L.P. Cao, J.Y. Zhang, G. Liu, B.A. Chen, J. Sun, The influence of Sc solute partitioning on the microalloying effect and mechanical properties of Al-Cu alloys with minor Sc addition, *Acta Mater.* 119 (2016) 68–79.

<https://doi.org/10.1016/j.actamat.2016.08.013>.

[155] Y. Zheng, Y. Liu, N. Wilson, S. Liu, X. Zhao, H. Chen, J. Li, Z. Zheng, L. Bourgeois, J.-F. Nie, Solute segregation induced sandwich structure in Al-Cu(-Au) alloys, *Acta Mater.* 184 (2020) 17–29. <https://doi.org/10.1016/j.actamat.2019.11.011>.

[156] J.D. Poplawsky, B.K. Milligan, L.F. Allard, D. Shin, P. Shower, M.F. Chisholm, A. Shyam, The synergistic role of Mn and Zr/Ti in producing $\theta'/\text{L1}(2)$ co-precipitates in Al-Cu alloys, *Acta Mater.* 194 (2020) 577–586. <https://doi.org/10.1016/j.actamat.2020.05.043>.

[157] L. Jiang, B. Rouxel, T. Langan, T. Dorin, Coupled segregation mechanisms of Sc, Zr and Mn at θ' interfaces enhances the strength and thermal stability of Al-Cu alloys, *Acta Mater.* 206 (2021) 116634. <https://doi.org/10.1016/j.actamat.2021.116634>.

[158] M.F. Chisholm, D. Shin, G. Duscher, M.P. Oxley, L.F. Allard, J.D. Poplawsky, A. Shyam, Atomic structures of interfacial solute gateways to θ' precipitates in Al-Cu alloys, *Acta Mater.* 212 (2021) 116891. <https://doi.org/10.1016/j.actamat.2021.116891>.

[159] E. Gumbmann, W. Lefebvre, F. De Geuser, C. Sigli, A. Deschamps, The effect of minor solute additions on the precipitation path of an Al-Cu-Li alloy, *Acta Mater.* 115 (2016) 104–114. <https://doi.org/10.1016/j.actamat.2016.05.050>.

[160] C.R. Hutchinson, X. Fan, S.J. Pennycook, G.J. Shiflet, On the origin of the high coarsening

- resistance of Ω plates in Al-Cu-Mg-Ag alloys, *Acta Mater.* 49 (2001) 2827–2841.
- [161] S.J. Kang, Y.-W. Kim, M. Kim, J.-M. Zuo, Determination of interfacial atomic structure, misfits and energetics of Omega phase in Al-Cu-Mg-Ag alloy, *Acta Mater.* 81 (2014) 501–511. <https://doi.org/10.1016/j.actamat.2014.07.074>.
- [162] B. Cheng, X. Zhao, Y. Zhang, H. Chen, I. Polmear, J.-F. Nie, Co-segregation of Mg and Zn atoms at the planar $\eta(1)$ -precipitate/Al matrix interface in an aged Al-Zn-Mg alloy, *Scr. Mater.* 185 (2020) 51–55. <https://doi.org/10.1016/j.scriptamat.2020.04.004>.
- [163] A.M. Cassell, J.D. Robson, X. Zhou, T. Hashimoto, M. Besel, The direct observation of copper segregation at the broad faces of η' and η precipitates in AA7010 aluminium alloy, *Mater. Charact.* 163 (2020) 110232. <https://doi.org/10.1016/j.matchar.2020.110232>.
- [164] Y. Weng, L. Ding, Z. Zhang, Z. Jia, B. Wen, Y. Liu, S. Muraishi, Y. Li, Q. Liu, Effect of Ag addition on the precipitation evolution and interfacial segregation for Al-Mg-Si alloy, *Acta Mater.* 180 (2019) 301–316. <https://doi.org/10.1016/j.actamat.2019.09.015>.
- [165] P. Pandey, S.K. Makineni, B. Gault, K. Chattopadhyay, On the origin of a remarkable increase in the strength and stability of an Al rich Al-Ni eutectic alloy by Zr addition, *Acta Mater.* 170 (2019) 205–217. <https://doi.org/10.1016/j.actamat.2019.03.025>.
- [166] C. Liu, H. Chen, J.-F. Nie, Interphase boundary segregation of Zn in Mg-Sn-Zn alloys, *Scr. Mater.* 123 (2016) 5–8. <https://doi.org/10.1016/j.scriptamat.2016.05.035>.
- [167] C.Q. Liu, H.W. Chen, N.C. Wilson, J.F. Nie, Zn segregation in interface between Mg₁₇Al₁₂ precipitate and Mg matrix in Mg-Al-Zn alloys, *Scr. Mater.* 163 (2019) 91–95. <https://doi.org/10.1016/j.scriptamat.2019.01.001>.
- [168] X. Gao, H. Wang, C. Ma, M. Lv, H. Ren, Segregation of alloying elements at the bcc-Fe/B2-NiAl interface and the corresponding effects on the interfacial energy, *Intermetallics*. 131 (2021) 107096. <https://doi.org/10.1016/j.intermet.2021.107096>.
- [169] T. Xi, X. Zhang, X. Yin, C. Yang, K. Yang, Interfacial segregation and precipitation behavior of Cu-rich precipitates in Cu-bearing 316LN stainless steel after aging at different temperatures, *Mater. Sci. Eng. -Struct. Mater. Prop. Microstruct. Process.* 805 (2021) 140571. <https://doi.org/10.1016/j.msea.2020.140571>.
- [170] D. Tytko, P.-P. Choi, J. Kloewer, A. Kostka, G. Inden, D. Raabe, Microstructural evolution of a Ni-based superalloy (617B) at 700 degrees C studied by electron microscopy and atom probe tomography, *Acta Mater.* 60 (2012) 1731–1740. <https://doi.org/10.1016/j.actamat.2011.11.020>.
- [171] L.T. Mushongera, M. Fleck, J. Kundin, Y. Wang, H. Emmerich, Effect of Re on directional γ' -coarsening in commercial single crystal Ni-base superalloys: A phase field study, *Acta Mater.* 93 (2015) 60–72. <https://doi.org/10.1016/j.actamat.2015.03.048>.
- [172] E.A. Lass, D.J. Sauza, D.C. Dunand, D.N. Seidman, Multicomponent γ' -strengthened Co-based superalloys with increased solvus temperatures and reduced mass densities, *Acta Mater.* 147 (2018) 284–295. <https://doi.org/10.1016/j.actamat.2018.01.034>.
- [173] D.J. Sauza, D.C. Dunand, D.N. Seidman, Microstructural evolution and high-temperature strength of a $\gamma(\text{f.c.c.})/\gamma'(L1(2))$ Co-Al-W-Ti-B superalloy, *Acta Mater.* 174 (2019) 427–438. <https://doi.org/10.1016/j.actamat.2019.05.058>.
- [174] O.R. Myhr, O. Grong, S.J. Andersen, Modelling of the age hardening behaviour of Al-Mg-Si alloys, *Acta Mater.* 49 (2001) 65–75.
- [175] J. da Costa Teixeira, D.G. Cram, L. Bourgeois, T.J. Bastow, A.J. Hill, C.R. Hutchinson, On the strengthening response of aluminum alloys containing shear-resistant plate-shaped precipitates, *Acta Mater.* 56 (2008) 6109–6122. <https://doi.org/10.1016/j.actamat.2008.08.023>.
- [176] B. Decreus, A. Deschamps, F. De Geuser, P. Donnadieu, C. Sigli, M. Weyland, The influence of Cu/Li ratio on precipitation in Al-Cu-Li-x alloys, *Acta Mater.* 61 (2013) 2207–2218.
- [177] A. Deschamps, M. Garcia, J. Chevy, B. Davo, F. De Geuser, Influence of Mg and Li content on the microstructure evolution of Al-Cu-Li alloys during long-term ageing, *Acta Mater.* 122 (2017) 32–46. <https://doi.org/10.1016/j.actamat.2016.09.036>.
- [178] P. Fratzl, F. Langmayr, O. Paris, EVALUATION OF 3D SMALL-ANGLE SCATTERING FROM NONSPHERICAL PARTICLES IN SINGLE-CRYSTALS, *J. Appl. Crystallogr.* 26 (1993)

820–826.

- [179] F. De Geuser, F. Bley, A. Deschamps, A new method for evaluating the size of plate-like precipitates by small-angle scattering, *J. Appl. Crystallogr.* 45 (2012) 1208–1218. <https://doi.org/10.1107/S0021889812039891>.
- [180] T. Dorin, A. Deschamps, F. De Geuser, C. Sigli, Quantification and modelling of the microstructure/strength relationship by tailoring the morphological parameters of the T1 phase in an Al–Cu–Li alloy, *Acta Mater.* 75 (2014) 134–146. <https://doi.org/10.1016/j.actamat.2014.04.046>.
- [181] C.S.T. Chang, F. De Geuser, J. Banhart, In situ characterization of beta ' ' precipitation in an Al-Mg-Si alloy by anisotropic small-angle neutron scattering on a single crystal, *J. Appl. Crystallogr.* 48 (2015) 455–463.
- [182] C. Hutchinson, J. Nie, S. Gorsse, Modeling the precipitation processes and strengthening mechanisms in a Mg-Al-(Zn) AZ91 alloy, *Metall. Mater. Trans. Phys. Metall. Mater. Sci.* 36A (2005) 2093–2105.
- [183] G. Rubin, A.G. Khachaturyan, Three-dimensional model of precipitation of ordered intermetallics, *Acta Mater.* 47 (1999) 1995–2002. [https://doi.org/10.1016/S1359-6454\(99\)00107-X](https://doi.org/10.1016/S1359-6454(99)00107-X).
- [184] K. Kim, A. Roy, M.P. Gururajan, C. Wolverton, P.W. Voorhees, First-principles/Phase-field modeling of similar to \) ' precipitation in Al-Cu alloys, *Acta Mater.* 140 (2017) 344–354. <https://doi.org/10.1016/j.actamat.2017.08.046>.
- [185] V. Vaithyanathan, C. Wolverton, L.Q. Chen, Multiscale modeling of theta ' precipitation in Al-Cu binary alloys, *Acta Mater.* 52 (2004) 2973–2987. <https://doi.org/10.1016/j.actamat.2004.03.001>.
- [186] J. Svoboda, F.D. Fischer, P.H. Mayrhofer, A model for evolution of shape changing precipitates in multicomponent systems, *Acta Mater.* 56 (2008) 4896–4904. <https://doi.org/10.1016/j.actamat.2008.06.016>.
- [187] D. Bardel, M. Perez, D. Nelias, A. Deschamps, C.R. Hutchinson, D. Maisonnette, T. Chaise, J. Garnier, F. Bourlier, Coupled precipitation and yield strength modelling for non-isothermal treatments of a 6061 aluminium alloy, *Acta Mater.* 62 (2014) 129–140. <https://doi.org/10.1016/j.actamat.2013.09.041>.
- [188] A. Balan, M. Perez, T. Chaise, S. Cazottes, D. Bardel, F. Corpacci, F. Pichot, A. Deschamps, F. De Geuser, D. Nelias, Precipitation of γ'' in Inconel 718 alloy from microstructure to mechanical properties, *Materialia*. 20 (2021) 101187. <https://doi.org/10.1016/j.mtla.2021.101187>.
- [189] B. Holmedal, E. Osmundsen, Q. Du, Precipitation of Non-Spherical Particles in Aluminum Alloys Part I: Generalization of the Kampmann-Wagner Numerical Model, *Metall. Mater. Trans. - Phys. Metall. Mater. Sci.* 47A (2016) 581–588. <https://doi.org/10.1007/s11661-015-3197-5>.
- [190] Q. Du, B. Holmedal, J. Friis, C.D. Marioara, Precipitation of Non-spherical Particles in Aluminum Alloys Part II: Numerical Simulation and Experimental Characterization During Aging Treatment of an Al-Mg-Si Alloy, *Metall. Mater. Trans. -Phys. Metall. Mater. Sci.* 47A (2016) 589–599. <https://doi.org/10.1007/s11661-015-3196-6>.
- [191] J.J. Hoyt, The velocity of plate precipitates growing by the ledge mechanism, *Acta Mater.* 61 (2013) 4953–4960. <https://doi.org/10.1016/j.actamat.2013.04.051>.
- [192] M. Gazizov, R. Kaibyshev, Precipitation structure and strengthening mechanisms in an Al-Cu-Mg-Ag alloy, *Mater. Sci. Eng. -Struct. Mater. Prop. Microstruct. Process.* 702 (2017) 29–40. <https://doi.org/10.1016/j.msea.2017.06.110>.
- [193] M. Perez, A. Deschamps, Microscopic modelling of simultaneous two-phase precipitation: application to carbide precipitation in low-carbon steels, *Mater. Sci. Eng. A.* 360 (2003) 214–219.
- [194] E. Povoden-Karadeniz, P. Lang, P. Warczok, A. Falahati, W. Jun, E. Kozeschnik, CALPHAD modeling of metastable phases in the Al–Mg–Si system, *Calphad.* 43 (2013) 94–104. <https://doi.org/10.1016/j.calphad.2013.03.004>.
- [195] O.R. Myhr, O. Grong, C. Schaefer, An Extended Age-Hardening Model for Al-Mg-Si Alloys Incorporating the Room-Temperature Storage and Cold Deformation Process Stages, *Metall. Mater. Trans. -Phys. Metall. Mater. Sci.* 46A (2015) 6018–6039. <https://doi.org/10.1007/s11661-015-3175-y>.

- [196] P. Lang, E. Povoden-Karadeniz, A. Falahati, E. Kozeschnik, Simulation of the effect of composition on the precipitation in 6xxx Al alloys during continuous-heating DSC, *J. Alloys Compd.* 612 (2014) 443–449. <https://doi.org/10.1016/j.jallcom.2014.05.191>.
- [197] G. Stechauner, E. Kozeschnik, Thermo-kinetic modeling of Cu precipitation in α -Fe, *Acta Mater.* 100 (2015) 135–146. <https://doi.org/10.1016/j.actamat.2015.08.042>.
- [198] J. Zhu, T. Zhang, Y. Yang, C.T. Liu, Phase field study of the copper precipitation in Fe-Cu alloy, *Acta Mater.* 166 (2019) 560–571. <https://doi.org/10.1016/j.actamat.2019.01.009>.
- [199] C.-S. Tsao, E.-W. Huang, M.-H. Wen, T.-Y. Kuo, S.-L. Jeng, U.-S. Jeng, Y.-S. Sun, Phase transformation and precipitation of an Al–Cu alloy during non-isothermal heating studied by in situ small-angle and wide-angle scattering, *J. Alloys Compd.* 579 (2013) 138–146. <https://doi.org/10.1016/j.jallcom.2013.04.201>.
- [200] S.J. Andersen, C.D. Marioara, J. Friis, S. Wenner, R. Holmestad, Precipitates in aluminium alloys, *Adv. Phys.-X.* 3 (2018) 790–813. <https://doi.org/10.1080/23746149.2018.1479984>.
- [201] A. Bendo, K. Matsuda, K. Nishimura, N. Nunomura, T. Tsuchiya, S. Lee, C.D. Marioara, T. Tsuru, M. Yamaguchi, K. Shimizu, H. Toda, The possible transition mechanism for the meta-stable phase in the 7xxx aluminium, *Mater. Sci. Technol.* 36 (2020) 1621–1627. <https://doi.org/10.1080/02670836.2020.1821323>.
- [202] Z.B. Jiao, J.H. Luan, M.K. Miller, C.Y. Yu, Y. Liu, C.T. Liu, Precipitate transformation from NiAl-type to Ni₂AlMn-type and its influence on the mechanical properties of high-strength steels, *Acta Mater.* 110 (2016) 31–43. <https://doi.org/10.1016/j.actamat.2016.03.024>.
- [203] C. Pareige, J. Emo, S. Sallet, C. Domain, P. Pareige, Kinetics of G-phase precipitation and spinodal decomposition in very long aged ferrite of a Mo-free duplex stainless steel, *J. Nucl. Mater.* 465 (2015) 383–389. <https://doi.org/10.1016/j.jnucmat.2015.06.017>.
- [204] C. Antion, P. Donnadiou, F. Perrard, A. Deschamps, C. Tassin, A. Pisch, Hardening precipitation in a Mg-4Y-3RE alloy, *ACTA Mater.* 51 (2003) 5335–5348. [https://doi.org/10.1016/S1359-6454\(03\)00391-4](https://doi.org/10.1016/S1359-6454(03)00391-4).
- [205] A. Sanaty-Zadeh, A.A. Luo, D.S. Stone, Comprehensive study of phase transformation in age-hardening of Mg–3Nd–0.2Zn by means of scanning transmission electron microscopy, *Acta Mater.* 94 (2015) 294–306. <https://doi.org/10.1016/j.actamat.2015.05.001>.
- [206] R. Shi, D.P. McAllister, N. Zhou, A.J. Detor, R. DiDomizio, M.J. Mills, Y. Wang, Growth behavior of gamma ' /gamma ' ' coprecipitates in Ni-Base superalloys, *Acta Mater.* 164 (2019) 220–236. <https://doi.org/10.1016/j.actamat.2018.10.028>.
- [207] B. Decreus, A. Deschamps, F. de Geuser, C. Sigli, Influence of Natural Ageing and Deformation on Precipitation in an Al–Cu–Li Alloy, *Adv. Eng. Mater.* 15 (2013) 1082–1085. <https://doi.org/10.1002/adem.201300098>.
- [208] C. Genevois, D. Fabrègue, A. Deschamps, W.J. Poole, On the coupling between precipitation and plastic deformation in relation with friction stir welding of AA2024 T3 aluminium alloy, *Mater. Sci. Eng. A.* 441 (2006) 39–48.
- [209] A. Chbihi, X. Sauvage, D. Blavette, Influence of plastic deformation on the precipitation of Cr in copper, *J. Mater. Sci.* 49 (2014) 6240–6247. <https://doi.org/10.1007/s10853-014-8348-3>.
- [210] B.I. Rodgers, P.B. Prangnell, Quantification of the influence of increased pre-stretching on microstructure-strength relationships in the Al-Cu-Li alloy AA2195, *Acta Mater.* 108 (2016) 55–67. <https://doi.org/10.1016/j.actamat.2016.02.017>.
- [211] A. Chbihi, S. Vincent, J. Ribis, C. Toffolon-Masclet, J. Garnier, Influence of plastic deformation on the precipitation sequence in an AA6061 alloy, *J. Mater. Sci.* 52 (2017) 6063–6073. <https://doi.org/10.1007/s10853-017-0845-8>.
- [212] B. Gwalani, S. Gorsse, D. Choudhuri, M. Styles, Y. Zheng, R.S. Mishra, R. Banerjee, Modifying transformation pathways in high entropy alloys or complex concentrated alloys via thermo-mechanical processing, *Acta Mater.* 153 (2018) 169–185. <https://doi.org/10.1016/j.actamat.2018.05.009>.
- [213] A. Deschamps, F. De Geuser, Z. Horita, S. Lee, G. Renou, Precipitation kinetics in a severely plastically deformed 7075 aluminium alloy, *Acta Mater.* 66 (2014) 105–117.

<https://doi.org/10.1016/j.actamat.2013.11.071>.

- [214] Y. Huang, J.D. Robson, P.B. Prangnell, The formation of nanograin structures and accelerated room-temperature θ precipitation in a severely deformed Al-4 wt.% Cu alloy, *Acta Mater.* 58 (2010) 1643–1657. <https://doi.org/10.1016/j.actamat.2009.11.008>.
- [215] Z.Q. Feng, Y.Q. Yang, B. Huang, X. Luo, M.H. Li, M. Han, M.S. Fu, Variant selection and the strengthening effect of θ precipitates at dislocations in Al-Cu-Mg alloy, *Acta Mater.* 59 (2011) 2412–2422. <https://doi.org/10.1016/j.actamat.2010.12.041>.
- [216] W.A. Cassada, G.J. Shiflet, E.A.J. Starke, The effect of plastic deformation on Al₂CuLi (T1) precipitation, *Metall. Trans. A.* 22A (1991) 299–306.
- [217] E. Dontsova, J. Rottler, C.W. Sinclair, Solute segregation kinetics and dislocation depinning in a binary alloy, *Phys. Rev. B.* 91 (2015) 224103. <https://doi.org/10.1103/PhysRevB.91.224103>.
- [218] H. Zhao, F. De Geuser, A.K. da Silva, A. Szczepaniak, B. Gault, D. Ponge, D. Raabe, Segregation assisted grain boundary precipitation in a model Al-Zn-Mg-Cu alloy, *Acta Mater.* 156 (2018) 318–329. <https://doi.org/10.1016/j.actamat.2018.07.003>.
- [219] A.K. da Silva, R.D. Kamachali, D. Ponge, B. Gault, J. Neugebauer, D. Raabe, Thermodynamics of grain boundary segregation, interfacial spinodal and their relevance for nucleation during solid-solid phase transitions, *Acta Mater.* 168 (2019) 109–120. <https://doi.org/10.1016/j.actamat.2019.02.005>.
- [220] L. Li, Z. Li, A.K. da Silva, Z. Peng, H. Zhao, B. Gault, D. Raabe, Segregation-driven grain boundary spinodal decomposition as a pathway for phase nucleation in a high-entropy alloy, *Acta Mater.* 178 (2019) 1–9. <https://doi.org/10.1016/j.actamat.2019.07.052>.
- [221] D.S. D'Antuono, J. Gaies, W. Golumbskie, M.L. Taheri, Direct measurement of the effect of cold rolling on beta phase precipitation kinetics in 5xxx series aluminum alloys, *Acta Mater.* 123 (2017) 264–271. <https://doi.org/10.1016/j.actamat.2016.10.060>.
- [222] N. Kamp, A. Sullivan, R. Tomasi, J.D. Robson, Modelling of heterogeneous precipitate distribution evolution during friction stir welding process, *Acta Mater.* 54 (2006) 2003–2014. <https://doi.org/10.1016/j.actamat.2005.12.024>.
- [223] F. Perrard, P. Donnadieu, A. Deschamps, P. Barges, TEM study of NbC heterogeneous precipitation in ferrite, *Philos. Mag.* 86 (2006) 4271–4284.
- [224] S. Zhang, J. Kohlbrecher, F.D. Tichelaar, G. Langelaan, E. Bruck, S. van der Zwaag, N.H. van Dijk, Defect-induced Au precipitation in Fe-Au and Fe-Au-B-N alloys studied by in situ small-angle neutron scattering, *ACTA Mater.* 61 (2013) 7009–7019. <https://doi.org/10.1016/j.actamat.2013.08.015>.
- [225] K. Teichmann, C.D. Marioara, S.J. Andersen, K. Marthinsen, The Effect of Preaging Deformation on the Precipitation Behavior of an Al-Mg-Si Alloy, *Metall. Mater. Trans. -Phys. Metall. Mater. Sci.* 43A (2012) 4006–4014. <https://doi.org/10.1007/s11661-012-1235-0>.
- [226] J. Robson, Extension of the N-model to predict competing homogeneous and heterogeneous precipitation in Al-Sc alloys, *Acta Mater.* 51 (2003) 1453–1468. [https://doi.org/10.1016/S1359-6454\(02\)00540-2](https://doi.org/10.1016/S1359-6454(02)00540-2).
- [227] F. Perrard, A. Deschamps, P. Maugis, Modelling the precipitation of NbC on dislocations in α -Fe, *Acta Mater.* 55 (2007) 1255–1266.
- [228] J.J. Hoyt, On the coarsening of precipitates located on grain boundaries and dislocations, *Acta Metall. Mater.* 39 (1991) 1091–2098.
- [229] N.J. Cunningham, M.J. Alinger, D. Klingensmith, Y. Wu, G.R. Odette, On nano-oxide coarsening kinetics in the nanostructured ferritic alloy MA957: A mechanism based predictive model, *Mater. Sci. Eng. -Struct. Mater. Prop. Microstruct. Process.* 655 (2016) 355–362. <https://doi.org/10.1016/j.msea.2015.12.074>.
- [230] Z.M. Wang, G.J. Shiflet, Heterogeneous nucleation of δ' on dislocations in a dilute aluminum-lithium alloy, *Metall. Mater. Trans. -Phys. Metall. Mater. Sci.* 27 (1996) 1599–1609. <https://doi.org/10.1007/BF02649818>.
- [231] F. Theska, K. Nomoto, F. Godor, B. Oberwinkler, A. Stanojevic, S.P. Ringer, S. Primig, On the early stages of precipitation during direct ageing of Alloy 718, *Acta Mater.* 188 (2020) 492–

503. <https://doi.org/10.1016/j.actamat.2020.02.034>.
- [232] E.I. Galindo-Nava, W.M. Rainforth, P.E.J. Rivera-Diaz-del-Castillo, Predicting microstructure and strength of maraging steels: Elemental optimisation, *Acta Mater.* 117 (2016) 270–285. <https://doi.org/10.1016/j.actamat.2016.07.020>.
- [233] W.Z. Han, Y. Chen, A. Vinogradov, C.R. Hutchinson, Dynamic precipitation during cyclic deformation of an underaged Al–Cu alloy, *Mater. Sci. Eng. A.* 528 (2011) 7410–7416. <https://doi.org/10.1016/j.msea.2011.06.037>.
- [234] C.R. Hutchinson, F. de Geuser, Y. Chen, A. Deschamps, Quantitative measurements of dynamic precipitation during fatigue of an Al–Zn–Mg–(Cu) alloy using small-angle X-ray scattering, *Acta Mater.* 74 (2014) 96–109. <https://doi.org/10.1016/j.actamat.2014.04.027>.
- [235] W. Sun, Y. Zhu, R. Marceau, L. Wang, Q. Zhang, X. Gao, C. Hutchinson, Precipitation strengthening of aluminum alloys by room-temperature cyclic plasticity, *Science*. 363 (2019) 972–975. <https://doi.org/10.1126/science.aav7086>.
- [236] Q. Zhang, Y. Zhu, X. Gao, Y. Wu, C. Hutchinson, Training high-strength aluminum alloys to withstand fatigue, *Nat. Commun.* 11 (2020) 5198. <https://doi.org/10.1038/s41467-020-19071-7>.
- [237] J. Zhou, J. Odqvist, A. Ruban, M. Thuvander, W. Xiong, J. Ågren, G.B. Olson, P. Hedström, Effect of solution treatment on spinodal decomposition during aging of an Fe–46.5 at.% Cr alloy, *J. Mater. Sci.* 52 (2017) 326–335. <https://doi.org/10.1007/s10853-016-0333-6>.
- [238] X. Xu, J.E. Westraadt, J. Odqvist, T.G.A. Youngs, S.M. King, P. Hedstrom, Effect of heat treatment above the miscibility gap on nanostructure formation due to spinodal decomposition in Fe–52.85 at.%Cr, *Acta Mater.* 145 (2018) 347–358. <https://doi.org/10.1016/j.actamat.2017.12.008>.
- [239] B. Milkereit, M.J. Starink, Quench sensitivity of Al–Mg–Si alloys: A model for linear cooling and strengthening, *Mater. Des.* 76 (2015) 117–129. <https://doi.org/10.1016/j.matdes.2015.03.055>.
- [240] M.J. Starink, B. Milkereit, Y. Zhang, P.A. Rometsch, Predicting the quench sensitivity of Al–Zn–Mg–Cu alloys: A model for linear cooling and strengthening, *Mater. Des.* 88 (2015) 958–971. <https://doi.org/10.1016/j.matdes.2015.09.058>.
- [241] P. Schloth, J.N. Wagner, J.L. Fife, A. Menzel, J.-M. Drezet, H. Van Swygenhoven, Early precipitation during cooling of an Al–Zn–Mg–Cu alloy revealed by in situ small angle X-ray scattering, *Appl. Phys. Lett.* 105 (2014) 101908. <https://doi.org/10.1063/1.4894768>.
- [242] P. Schloth, A. Menzel, J.L. Fife, J.N. Wagner, H. Van Swygenhoven, J.-M. Drezet, Early cluster formation during rapid cooling of an Al–Cu–Mg alloy: In situ small-angle X-ray scattering, *Scr. Mater.* 108 (2015) 56–59. <https://doi.org/10.1016/j.scriptamat.2015.06.015>.
- [243] R. Radis, M. Schaffer, M. Albu, G. Kothleitner, P. Poelt, E. Kozeschnik, Multimodal size distributions of gamma ' precipitates during continuous cooling of UDIMET 720 Li, *Acta Mater.* 57 (2009) 5739–5747. <https://doi.org/10.1016/j.actamat.2009.08.002>.
- [244] G. Botissinot, A. Finel, Y. Le Bouar, Phase-field modeling of bimodal microstructures in nickel-based superalloys, *Acta Mater.* 57 (2009) 921–931. <https://doi.org/10.1016/j.actamat.2008.10.039>.
- [245] S. Luo, G. Wang, Y. Hu, Y. Zhong, Y. Rong, Effect of quenching rate and its coupling model on precipitation and strength of Al–Cu–Cd alloys, *Mater. Sci. Eng. A.* 761 (2019) 138022. <https://doi.org/10.1016/j.msea.2019.06.032>.
- [246] A. Deschamps, G. Texier, S. Ringeval, L. Delfaut-Durut, Influence of cooling rate on the precipitation microstructure in a medium strength Al–Zn–Mg alloy, *Mater. Sci. Eng. -Struct. Mater. Prop. Microstruct. Process.* 501 (2009) 133–139. <https://doi.org/10.1016/j.msea.2008.09.067>.
- [247] M. Tiryakioglu, J.S. Robinson, P.D. Eason, On the quench sensitivity of 7010 aluminum alloy forgings in the overaged condition, *Mater. Sci. Eng. -Struct. Mater. Prop. Microstruct. Process.* 618 (2014) 22–28. <https://doi.org/10.1016/j.msea.2014.09.002>.
- [248] C.P. Massey, S.N. Dryepontd, P.D. Edmondson, M.G. Frith, K.C. Littrell, A. Kini, B. Gault, K.A. Terrani, S.J. Zinkle, Multiscale investigations of nanoprecipitate nucleation, growth, and coarsening in annealed low-Cr oxide dispersion strengthened FeCrAl powder, *Acta Mater.* 166 (2019) 1–17. <https://doi.org/10.1016/j.actamat.2018.11.062>.

- [249] Y. Chen, M. Weyland, C.R. Hutchinson, The effect of interrupted aging on the yield strength and uniform elongation of precipitation-hardened Al alloys, *Acta Mater.* 61 (2013) 5877–5894. <https://doi.org/10.1016/j.actamat.2013.06.036>.
- [250] C.R. Hutchinson, M. Goune, A. Redjaimia, Selecting non-isothermal heat treatment schedules for precipitation hardening systems: An example of coupled process-property optimization, *Acta Mater.* 55 (2007) 213–223. <https://doi.org/10.1016/j.actamat.2006.07.028>.
- [251] L. Shi, K. Baker, R. Young, J. Kang, J. Liang, B. Shalchi-Amirkhiz, B. Langelier, Y. Brechet, C. Hutchinson, H. Zurob, The effect of chemical patterning induced by cyclic plasticity on the formation of precipitates during aging of an Al-Mg-Si alloy, *Mater. Sci. Eng. -Struct. Mater. Prop. Microstruct. Process.* 815 (2021) 141265. <https://doi.org/10.1016/j.msea.2021.141265>.
- [252] A. Deschamps, F. Livet, Y. Brechet, Influence of predeformation on ageing in an Al-Zn-Mg alloy - I. Microstructure evolution and mechanical properties, *Acta Mater.* 47 (1999) 281–292.
- [253] Y. Takaki, T. Masuda, E. Kobayashi, T. Sato, Effects of Natural Aging on Bake Hardening Behavior of Al-Mg-Si Alloys with Multi-Step Aging Process, *Mater. Trans.* 55 (2014) 1257–1265. <https://doi.org/10.2320/matertrans.L-M2014827>.
- [254] O. Engler, C.D. Marioara, Y. Aruga, M. Kozuka, O.R. Myhr, Effect of natural ageing or pre-ageing on the evolution of precipitate structure and strength during age hardening of Al-Mg-Si alloy AA 6016, *Mater. Sci. Eng. A.* 759 (2019) 520–529. <https://doi.org/10.1016/j.msea.2019.05.073>.
- [255] G. Fribourg, A. Deschamps, Y. Brechet, G. Mylonas, G. Labeas, U. Heckenberger, M. Perez, Microstructure modifications induced by a laser surface treatment in an AA7449 aluminium alloy, *Mater. Sci. Eng. -Struct. Mater. Prop. Microstruct. Process.* 528 (2011) 2736–2747. <https://doi.org/10.1016/j.msea.2010.12.018>.
- [256] B. Wahlmann, F. Galgon, A. Stark, S. Gayer, N. Schell, P. Staron, C. Koerner, Growth and coarsening kinetics of gamma prime precipitates in CMSX-4 under simulated additive manufacturing conditions, *Acta Mater.* 180 (2019) 84–96. <https://doi.org/10.1016/j.actamat.2019.08.049>.
- [257] M. Nicolas, A. Deschamps, Characterisation and modelling of precipitate evolution in an Al-Zn-Mg alloy during non-isothermal heat treatments, *Acta Mater.* 51 (2003) 6077–6094.
- [258] A. Deschamps, C. Genevois, M. Nicolas, F. Perrard, F. Bley, Study of precipitation kinetics: towards non-isothermal and coupled phenomena, *Philos. Mag.* 85 (2005) 3091–3112. <https://doi.org/10.1080/14786430500154513>.
- [259] A. Deschamps, M. Perez, Mesoscopic modelling of precipitation: A tool for extracting physical parameters of phase transformations in metallic alloys, *C R Phys.* 11 (2010) 236–244.
- [260] A. Deschamps, C. Sigli, T. Mourey, F. de Geuser, W. Lefebvre, B. Davo, Experimental and modelling assessment of precipitation kinetics in an Al-Li-Mg alloy, *Acta Mater.* 60 (2012) 1917–1928. <https://doi.org/10.1016/j.actamat.2012.01.010>.
- [261] M. Nicolas, A. Deschamps, Precipitate microstructures and resulting properties of Al-Zn-Mg MIG-weld heat affected zones, *Metall. Mater. Trans.* 35A (2004) 1437–1448.